NACA TN 2488

NATIONAL ADVISORY COMMITTEE FOR AERONAUTICS

TECHNICAL NOTE 2488

WIND-TUNNEL INVESTIGATION OF THE CONTRIBUTION OF A VERTICAL TAIL TO THE DIRECTIONAL STABILITY OF A FIGHTER-TYPE AIRPLANE

By Alfred A. Marino and N. Mastrocola

Langley Aeronautical Laboratory
Langley Field, Va.

Washington
January 1952

1R

NATIONAL ADVISORY COMMITTEE FOR AERONAUTICS

TECHNICAL NOTE 2488

WIND-TUNNEL INVESTIGATION OF THE CONTRIBUTION OF A VERTICAL TAIL TO THE DIRECTIONAL STABILITY OF A FIGHTER-TYPE AIRPLANE[1]

By Alfred A. Marino and N. Mastrocola

SUMMARY

Tests of a $\frac{1}{3}$-scale model of a typical fighter-type airplane were made to investigate the contribution of a centrally located vertical tail to the directional stability. Propeller-removed tests were made with the stabilizer located in three vertical positions on the fuselage. The separate contributions of the tail and the fuselage were determined by means of pressure measurements on the tail and on the fuselage in the vicinity of the tail.

The results of the tests indicated that the stabilizer, apart from its favorable end-plate effect, had a large detrimental effect on the contribution of the vertical tail surface to the directional stability. This detrimental effect was greatest with the stabilizer high on the fuselage and increased with increasing angle of attack. The contribution of the fuselage at small angles of attack was supplied mainly by that part above the stabilizer. The importance of the contribution of this part of the fuselage increased considerably as the stabilizer was moved down. The contribution of the fuselage below the stabilizer was negligible at small angles of attack; at high angles of attack the contribution of the fuselage became appreciable when the depth of the fuselage below the stabilizer was large.

A comparison of the test results with results predicted by two different design methods based on the concept of an effective tail area indicates that such methods cannot accurately predict the contribution of a vertical tail to the directional stability for all airplane configurations and flight conditions. It appears that, for airplanes with tail configurations similar to the type investigated, a more satisfactory method can be obtained by treating separately the contributions of the

---

[1]Supersedes the recently declassified RM L7K03, "Wind-Tunnel Investigation of the Contribution of a Vertical Tail to the Directional Stability of a Fighter-Type Airplane" by Alfred A. Marino and N. Mastrocola, 1948.

vertical tail surface, the fuselage area above the stabilizer, and the fuselage area below the stabilizer.

INTRODUCTION

Two widely accepted available methods for predicting the contribution of a vertical tail to the directional stability (references 1 and 2) involve tail-area definitions that include part of the lateral area of the fuselage. The two tail-area definitions, however, are not the same, and the two methods do not give consistent results. Recent tests (reference 3) disclosed a lack of agreement between experimental results and those results predicted by reference 1 and indicated that the vertical tail and fuselage should be considered separately inasmuch as sidewash and dynamic-pressure measurements indicated that the loading on the after part of the fuselage was not changed appreciably by the addition of the vertical tail. The present investigation of a $\frac{1}{3}$-scale model of the fighter-type airplane tested in reference 3 was conducted in the Langley propeller-research tunnel to determine the separate contributions of the fuselage and vertical tail surface to the directional stability and to study the applicability of current design methods. Inasmuch as all tests were made with propeller removed, the effects of propeller slipstream were not considered in this investigation.

The data were obtained by means of pressure orifices installed on the vertical tail and on the fuselage in the region of the vertical tail; thereby, the separate determination of the loads on the tail and fuselage was possible. Pressure measurements on the fuselage were taken with the vertical tail both on and off so that the load induced by the vertical tail could be determined. Three vertical positions of the stabilizer on the fuselage were investigated. The tests were made for a range of angle of yaw from 0° to 25° and a range of angle of attack from 0° to 15°.

SYMBOLS

A	geometric aspect ratio
A_e	effective aspect ratio
C_L	lift coefficient $\left(L/q_\infty S\right)$
C_n	yawing-moment coefficient $\left(N/q_\infty Sb\right)$
L	force perpendicular to free stream; positive when acting upward

N	yawing moment about lift axis; positive when nose tends to turn to right
S_w	wing area, 37.1 square feet
S_t	tail area
l	distance from center of gravity to rudder hinge line, 7.25 feet
b	wing span, 14.27 feet
h_t	height of vertical tail
c	chord of vertical tail or fuselage
c_n	section normal-force coefficient
c_{n_t}	section normal-force coefficient on vertical tail or on fuselage due to vertical tail
C_N	normal-force coefficient on vertical tail or on fuselage due to vertical tail (based on vertical-tail area) $(N_t/q_o S_t)$
N_t	normal force on vertical tail or on fuselage due to vertical tail
α	angle of attack of fuselage reference line with respect to axis of wind tunnel, degrees
α_c	angle of attack corrected for jet-boundary effects, degrees
ψ	angle of yaw, degrees; positive when left wing is forward
σ	sidewash angle, degrees; positive when flow is from right to left when airplane is viewed from rear
q	local dynamic pressure
q_o	free-stream dynamic pressure
y	spanwise position measured vertically from fuselage reference line, inches (see fig. 3)
C_{N_ψ}	rate of change of C_N with ψ, per degree $\left(dC_N/d\psi\right)$
C_{n_ψ}	rate of change of C_n with ψ, per degree $(dC_n/d\psi)$

Subscripts:

t tail

w wing

MODEL AND TESTS

The tests were conducted on a $\frac{1}{3}$-scale model of a conventional low-wing fighter airplane. A three-view drawing showing the principal dimensions and areas is given as figure 1 and a photograph of the model mounted for testing is presented as figure 2. The most significant feature of the fuselage pertaining to this investigation is the great depth and wedge shape of the fuselage where the vertical tail is situated. Some of the details of the airplane, such as cowl flaps, propeller, and landing gear, were not represented on the model and the vertical tail and stabilizer were made without control surfaces.

The vertical tail, details of which are given in figure 3, was instrumented with surface pressure orifices distributed over both sides as shown in figure 4. Orifices were also installed in the rear part of of the fuselage directly below the vertical tail. The horizontal tail (fig. 5) was mounted in the three vertical positions shown in figure 3. For some tests, the horizontal tail was removed. Tail-off tests were made with both the horizontal and vertical tail surfaces removed. The vertical tail surface is defined as the part of the lateral area above the upper contour of the fuselage. (See fig. 2.)

The model was mounted on a single strut so that the only restraint about the vertical axis passing through the support point was a cantilever spring upon which were mounted electrical strain gages calibrated to measure the yawing tendency of the model. In addition six-component force measurements were obtained by means of the balance system of the Langley propeller-research tunnel.

All tests were made with propeller removed at a tunnel airspeed of approximately 80 miles per hour, corresponding to a Reynolds number of about 2×10^6 based on the mean wing chord. All tests were made for a range of angle of yaw from 0° to 25° and a range of angle of attack from 0° to 15°.

RESULTS

In order to simplify the presentation of results, the angles of attack for all the figures and throughout the text are uncorrected for wind-tunnel jet-boundary effect. The corrected angles of attack, together with the corresponding lift coefficients, are given in the following table for all conditions tested:

α (deg)	α_c (deg)	C_L	
		Stabilizer on	Stabilizer removed
0	-0.2	0.18	0.16
3	2.7	.37	.34
6	5.5	.57	.52
9	8.3	.76	.70
12	11.2	.96	.89
15	14.0	1.16	1.07

Pressures measured at the orifices on the vertical tail and fuselage were first plotted, in terms of the free-stream dynamic pressure, against the chordwise location. The areas enclosed by these curves from the leading edge to the trailing edge were mechanically integrated to give the section normal-force coefficient. The leading-edge limit for the integration of pressures on the fuselage was formed by the extension of the leading edge of the vertical tail through the fuselage as shown in figure 4; the section normal-force coefficient of the fuselage is thus based on a fictitious chord extending from the end of the fuselage to this boundary. The use of this chord was justified since the pressures at orifices located forward of this boundary were not changed appreciably by the installation or the removal of the vertical tail.

The fuselage section normal-force coefficients c_n measured with the vertical tail and stabilizer off are shown in figure 6. Values of c_{n_t}, the difference in section normal-force coefficient with the vertical tail on and off, are shown plotted against spanwise position in figure 7 for all conditions tested. For the case of the tail surface, these values are measures of the total load; whereas for the fuselage, these values are measures of the load induced on the fuselage by the vertical tail. For the low stabilizer position only the loading above the stabilizer was considered inasmuch as the load induced on the fuselage below the stabilizer was assumed to be negligibly small.

The net section normal-force coefficients c_{n_t} were multiplied by the local chord and plotted against the spanwise station to give the normal-force load distribution along the tail and the fuselage due to the addition of the vertical tail. These load curves are separated into sections as determined by the fuselage line and the horizontal-tail position. (See fig. 3.) The total load is thus interpreted as consisting of three parts: the load on the tail, the load on the fuselage above the stabilizer, and the load on the fuselage below the stabilizer. The areas under the load curves integrated between the specified boundaries are measures of the contributions of the component parts of the tail-fuselage combination to the total normal force due to the vertical tail; and since shifts in the position of the center of pressure are small in comparison with the tail length, these integrated values may also be considered proportional to the resulting yawing moment. Plots of the coresponding normal-force coefficients based on the area of the vertical tail surface, C_N against the angle of yaw ψ (fig. 8), show the contribution of the components of the tail-fuselage combination to the directional stability. The total yawing moment and lateral force produced by the vertical tail, calculated from the total normal-force coefficients shown in figure 8, were found to be in fair agreement with those measured directly by means of the strain gages and the tunnel scales.

Since the normal-force coefficient C_N is considered proportional to the yawing-moment coefficient C_n, the normal-force coefficient slope C_{N_ψ} is similarly proportional to the directional-stability derivative C_{n_ψ}. The slope of the normal-force curve for a component part of the tail-fuselage combination is thus a direct measure of the contribution of that part to the directional-stability derivative. The analysis in this paper is based on the average normal-force slope taken between $\psi = 0^\circ$ and 5°.

DISCUSSION

Throughout this paper the term "tail" is synonomous with the term "vertical tail" and is used to signify that part of the tail-fuselage combination removed in the tail-off tests, as described in the section entitled "Model and Tests." A distinction is also made between the expression "contribution of the vertical tail surface," which applies to the force acting on the vertical tail itself, and the expression "total contribution of the vertical tail," which applies to the total increment of force produced by the addition of the vertical tail.

Analysis of Experimental Results

Contribution of vertical tail surface.- The normal-force slopes for components of the tail-fuselage combinations obtained with the three stabilizer positions are shown in figure 9 plotted against angle of attack. The variations of these slopes with stabilizer position are shown in figure 10.

The data in figures 9 and 10 show that the stabilizer position has appreciable influence on the normal-force slope of the vertical tail surface. At $\alpha = 0^\circ$ the slopes obtained with the stabilizer in all positions tested are greater than the slope obtained with the stabilizer removed. The increase in tail slope for $\alpha = 0^\circ$ is attributable to the end-plate effect of the stabilizer. For the high-stabilizer position the increase in slopes produced by the end-plate effect of the stabilizer is reduced to zero at an angle of attack of about 3°, and as the angle of attack is increased, the slope is progressively decreased below that obtained with the stabilizer removed. For the middle and low stabilizer positions, the increase in slope produced by the end-plate effect is also reduced to zero but at the much higher angle of attack of 11°. These results indicate that at moderate and high angles of attack, the stabilizer has a detrimental effect on the tail effectiveness that outweighs its favorable end-plate effect. This detrimental effect increases with angle of attack and is greatest with the stabilizer in the high position.

The action in decreasing the contribution of the vertical tail surface can be attributed to an asymmetrical loading of the stabilizer due to the asymmetrical downwash behind the yawed airplane. The vortex system associated with such a loading results in a sidewash on the vertical tail that increases with angle of yaw and thus influences the effectiveness of the vertical tail. Whether the sidewash so produced is stabilizing or destabilizing depends upon the nature of the asymmetrical loading; in the present case, the action is clearly destabilizing. This effect is expected to vary with angle of attack, since its severity depends on the downwash asymmetry which is determined by the location of the stabilizer in the downwash pattern behind the wing. For the same reason, the effect would also vary with stabilizer position. This effect of the stabilizer is confined to small angles of yaw where the slopes of the normal-force curves are measured. At high angles of yaw the normal-force coefficients are larger with stabilizer than without (fig. 8), which indicates that the detrimental effect of the stabilizer is much less than its favorable end-plate effect.

It appears then that the presence of the stabilizer introduces two separate effects that influence the contribution of the vertical tail surface: the end-plate effect and the sidewash effect resulting from the asymmetrical stabilizer loading. The end-plate effect is due solely

to the interaction of vertical tail and stabilizer and is equivalent to an increase in the aspect ratio of the vertical tail. The sidewash effect is essentially independent of the presence of the vertical tail, because the sidewash would occur in this region even though the vertical tail were removed, and is properly treated in the same manner as the sidewash produced by the wing or fuselage or any other part of the airplane.

Although the stabilizer affects the direction of air flow at the vertical tail, the general characteristics of the air flow are primarily determined by the wing and fuselage. For this reason, the tail normal-force curves for the different stabilizer configurations are found to have the same general character. For small angles of yaw, the tail normal-force curves of figure 8 show a decrease in slope which becomes more pronounced as the angle of attack is increased. This trend is in accord with the air-flow measurements made in reference 3 where at small angles of yaw large losses in dynamic pressure resulting from the wakes of the canopy and wing-fuselage juncture were found to occur in the vicinity of the vertical tail. These losses increased with angle of attack because of the broadening of the wake but were less important at the higher angles of yaw where the tail moved out of the wake. The fuselage boundary layer reduces the dynamic pressure at the base of the vertical tail and therefore contributes to the sharp drop in load at that point. (See fig. 7.)

The normal-force-coefficient slope for the tail can be expressed as

$$C_{N_{\psi t}} = \left(C_{N_{\psi t}}\right)_o \frac{d(\psi - \sigma)(q/q_o)}{d\psi}$$

where $\left(C_{N_{\psi t}}\right)_o$ is the normal-force-coefficient slope of the tail for free-stream conditions ($\sigma = 0^\circ$ and $q = q_o$) and includes the end-plate effect of the stabilizer. Previous discussion shows that the factor $\frac{d(\psi - \sigma)(q/q_o)}{d\psi}$ is influenced by the stabilizer and varies with stabilizer position. The end-plate factor for the high-stabilizer position, calculated in table I on the basis of the corresponding air-flow measurements of reference 3, was 1.42 for an angle of attack of 0°. At intermediate angles of attack this value reduced to about 1.05 and then increased to a value of 1.48 at $\alpha = 15^\circ$ (fig. 11). The reduction of the end-plate factor at the intermediate angles of attack is believed to be caused by the passage of the stabilizer through the wake of the wing.

Contribution of fuselage above stabilizer.- The span-load curves of figure 7 show that the loading on the vertical tail decreases rapidly near the base of the vertical tail; the induced loading on the fuselage also decreases, but less rapidly, in going from the vertical-tail-fuselage juncture to the stabilizer. The stabilizer generally has the effect of increasing the intensity of load on the fuselage above the stabilizer over that existing with the stabilizer removed. The importance of the contribution of this part of the fuselage increases considerably as the stabilizer is moved down. (See fig. 10.) The contribution is only 5 percent of the total for the high-stabilizer position, but with the low-stabilizer position the contribution increases up to 20 percent of the total contribution of the vertical tail.

The curves of normal-force coefficient (fig. 8) show that the loading on the fuselage above the stabilizer increases almost linearly with angle of yaw. The curves show a decreased slope at small angles of yaw, which is similar to the behavior of the tail normal-force curves. This characteristic arises from the same cause, that is, the influence of wake at small angles of yaw. The small decrease of the slopes with angle of attack is also parallel to the trends exhibited by the tail normal-force-coefficient curves. In these respects, this part of the fuselage acts as a vertical-tail extension of reduced effectiveness.

Contribution of fuselage below stabilizer.- With the stabilizer removed, the induced load on the fuselage decreases continuously from the vertical-tail-fuselage juncture to the bottom of the fuselage. (See fig. 7(d).) With the stabilizer in place, the load on the fuselage decreases at a slower rate to the stabilizer. Across the stabilizer a sharp decrease in load occurs, and at high angles of yaw the direction of the induced normal force on the fuselage below the stabilizer is reversed. (See figs. 7(a) and 7(b).) The slopes of the curves of normal-force coefficient plotted against angle of yaw (fig. 8) are positive at small angles of yaw but become negative as the angle of yaw increases. The slopes of the curves tend to become more positive with increasing angle of attack, but at higher angles of yaw the characteristic trend remains an unstable one at all angles of attack.

The contribution of the fuselage below the stabilizer is negligible at small angles of attack as shown in figures 9 and 10. At high angles of attack the contribution of the fuselage becomes appreciable when the depth of the fuselage below the stabilizer is large. With the high stabilizer and at $\alpha = 15^{\circ}$, the contribution of this part of the fuselage is over 20 percent of the total contribution of the vertical tail.

Comparison with Conventional Design Methods

An examination of the methods of references 1 and 2 for predicting the increment in the directional stability produced by a vertical tail can now be evaluated on the basis of the results obtained in this investigation. The direct comparison between the measured results and those calculated are made only for the case of an angle of attack of 0°, since the facts brought out apply to all angles.

Pass' method.- Calculations of the contribution of the vertical tail to the directional-stability derivatives by the method of reference 1 are presented in table II for the three stabilizer positions tested. The air-flow factor measured with the high stabilizer in reference 3 was applied to all stabilizer positions. Although the results of this investigation indicated that this factor might vary with stabilizer position, its use for all positions is justified in these calculations since in the analysis of reference 1 no distinction is made for this effect of the stabilizer. The results of the calculations are shown plotted against stabilizer position in figure 12 in comparison with the experimental results. It is seen that the method of reference 1 leads to an overestimation that increases greatly as the stabilizer is moved down on the fuselage.

The reasons for the discrepancies between the measured and calculated results are disclosed by a careful examination of the procedure and of the assumptions involved in the method. The vertical-tail area in reference 1, as shown in the sketch in table II, is defined as the sum of the exposed vertical-tail area and that part of the fuselage immediately above the stabilizer, and the tail height is defined as the distance from the stabilizer to the tip of the vertical tail. The geometric aspect ratio of this plan form is then multiplied by a factor of 1.55 to account for the end-plate effect of the stabilizer. This aspect-ratio correction is almost the same as that found theoretically for the effective increase in aspect ratio of a vertical tail with a stabilizer at its base (reference 4). Therefore, Pass implies that the load on the tail-fuselage combination is almost the same as the load on an isolated vertical tail and stabilizer.

Theoretical load distributions for the isolated-tail configurations that apply to this model according to the method of reference 1 are shown in figure 13 for high- and low-stabilizer positions. These curves were determined from a series of load distributions derived theoretically in reference 4 for tails of elliptical plan form with stabilizers at their bases and are roughly corrected for the variation of sidewash and dynamic pressure by multiplying the load along the span by the air-flow factor used in table II. Although not exact, these load curves are considered accurate enough for purposes of illustration. The measured

span-load distributions for the vertical tail surface and fuselage above the stabilizer are also shown in figure 13. Since the loads are proportional to the angle of yaw, any differences in the areas under the measured and calculated curves are responsible for the differences in the measured and calculated directional-stability derivatives.

The most striking differences between the distributions of figure 13 occur on the fuselage where the actual loading is much lower than the calculated loading which continues essentially undiminished to the stabilizer. The contribution of the fuselage is thus overestimated; the error involved increases as the stabilizer is moved down. Another discrepancy, which also increases as the stabilizer is moved down, is the increased load on the tail itself which results from the increased geometric aspect ratio involved in the tail-area definition.

Agreement can be obtained between the calculated and experimental results by suitable readjustments of the end-plate factor, that is, readjustments of the effective aspect ratio. Calculations of the aspect-ratio correction factor required to give agreement showed that the factor would be about 1.00 for the high stabilizer and 0.60 for the low stabilizer as compared to 1.55 used by Pass for both cases. The use of such factors, however, is regarded as unjustifiable because the significance of this aspect-ratio correction as an end-plate effect is totally lost.

The previous discussion indicates that the use of the tail-area definition of reference 1 is generally inconsistent with observed results. For airplane configurations with high stabilizers, the induced loading on the fuselage above the stabilizer is not greatly different from that implied in the method, and with some modification of the end-plate factor, the method could give good results. It is pointed out, however, that, even in these cases, neglect of the fuselage below the stabilizer will lead to inaccurate results at high angles of attack.

Lyons and Bisgood's method.- Another method of vertical-tail design which involves a tail-area definition that includes all the fuselage area below the root chord of the vertical tail has been evolved by Lyons and Bisgood in reference 2. The calculations of the total effectiveness of the vertical tail according to this method are shown in table III. The results obtained are seen to be larger than the measured values (fig. 12).

In order to analyze the reasons for the large differences between the results shown in figure 12, the calculated total contribution is divided into the separate contributions of the tail, the fuselage above the stabilizer, and the fuselage below the stabilizer. For comparison

with the measured values, the contributions are taken as the normal-force-coefficient slopes, based on the tail area S_t, and are determined as shown in table IV by the relation

$$C_{N_\psi}{}_{component} = C_{N_\psi}{}_{total} \frac{S_{component}}{S_{total}}$$

This operation, although not strictly valid, is adequate for purposes of illustration, since the treatment of the tail and fuselage as a single airfoil implies a distribution of normal force that is roughly proportional to the areas involved.

The comparison of calculated results with the measured contributions of the components of the tail-fuselage combination is shown in figure 14. The most striking discrepancy is seen to lie in the large overestimation of the contribution of the fuselage. Inclusion in the tail area of the fuselage below the stabilizer, for which the contribution in the actual case was found to be zero, leads to a large and entirely fictitious contribution. The calculated contributions of the fuselage above the stabilizer, although more in accordance with the actual case, are still of questionable value due to an overestimation that increases greatly as the stabilizer is moved down. From consideration of the results obtained in this investigation it appears that a design method based on a tail-area definition as employed in reference 2 would tend to overestimate the contribution of the vertical tail for airplane tail configurations contributing relatively large fuselage area to the total effective tail area.

CONCLUSIONS

The results of the wind-tunnel investigation of the contribution of a vertical tail to the directional stability of a fighter-type airplane indicated that the stabilizer, apart from its favorable end-plate effect, had a large detrimental effect on the contribution of the vertical tail surface to the directional stability. This detrimental effect increased with angle of attack and was greatest with the stabilizer in the high position. The contribution of the fuselage at small angles of attack was supplied mainly by that part above the stabilizer. The importance of the contribution of this part of the fuselage increased appreciably as the stabilizer was moved down. The contribution of the fuselage below the stabilizer was negligible at small angles of attack; at high angles of attack, the contribution of the fuselage became appreciable when the depth of the fuselage below the stabilizer was large.

Inasmuch as the induced load on the fuselage contributes appreciably to the total effectiveness of the vertical tail, current design methods

generally attempt to account for this effect by including a part of the lateral area of the fuselage in this definition of the effective tail area. A comparison of the test results with results predicted by current design methods based on the concept of an effective tail area indicates that such methods cannot accurately predict the contribution of a vertical tail to the directional stability for all airplane configurations and flight conditions. It appears that a more satisfactory method can be obtained by treating separately the contributions of the vertical tail surface, the fuselage area above the stabilizer, and the fuselage area below the stabilizer.

Langley Aeronautical Laboratory
National Advisory Committee for Aeronautics
Langley Field, Va., December 9, 1947

REFERENCES

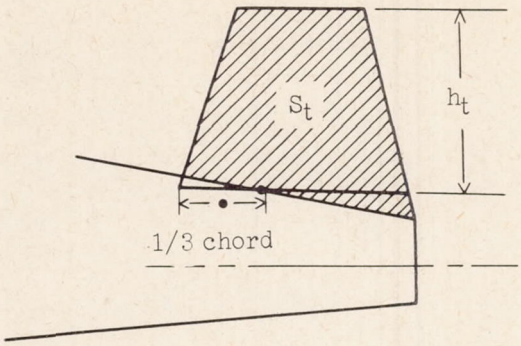
1. Pass, H. R.: Analysis of Wind-Tunnel Data on Directional Stability and Control. NACA TN 775, 1940.

2. Lyons, D. J., and Bisgood, P. L.: An Analysis of the Lift Slope of Aerofoils of Small Aspect Ratio, Including Fins, with Design Charts for Aerofoils and Control Surfaces. R. & M. No. 2308, British A.R.C., 1945.

3. Sweberg, Harold H., Guryansky, Eugene R., and Lange, Roy H.: Langley Full-Scale Tunnel Investigation of the Factors Affecting the Directional Stability and Trim Characteristics of a Fighter-Type Airplane. NACA ARR L5H09, 1945.

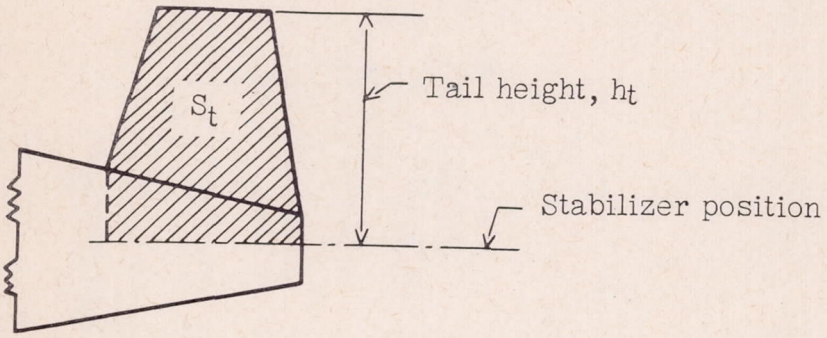
4. Katzoff, S., and Mutterperl, William: The End-Plate Effect of a Horizontal-Tail Surface on a Vertical-Tail Surface. NACA TN 797, 1941.

TABLE I.- CALCULATIONS OF END-PLATE FACTORS FOR VERTICAL TAIL



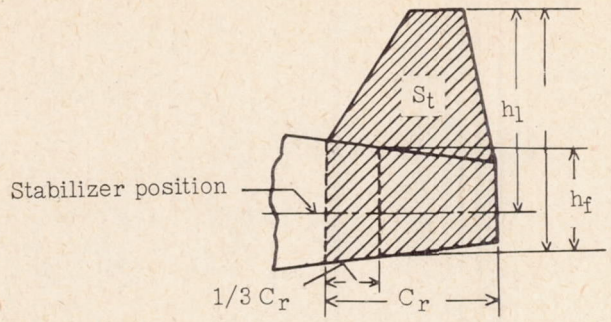
Angle of attack, α, deg	0	3	6	9	12	15
Area, S_t, sq ft	2.04					
Tail height, h_t, ft	1.55					
Aspect ratio, $A = h_t^2/S_t$	1.18					
Measured normal-force-coefficient slope for vertical tail surface (based on area S_t), $C_{N_{\psi_t}}$	0.0385	0.0330	0.0280	0.0255	0.0235	0.0210
Air-flow factor, $\frac{d(\psi - \sigma)(q/q_o)}{d\psi}$ (from reference 3 at same lift coefficient)	0.94	0.92	0.85	0.76	0.63	0.50
Corrected normal-force-coefficient slope, $\left(C_{N_{\psi_t}}\right)_o = \frac{C_{N_{\psi_t}}}{\text{Air-flow factor}}$ . .	0.0410	0.0360	0.0330	0.0336	0.0374	0.0420
Effective aspect ratio, A_e (from fig. 3 of reference 1 with values of $\left(C_{N_{\psi_t}}\right)_o$ decreased 5 percent to account for absence of control-surface gap)	1.68	1.39	1.22	1.26	1.46	1.75
End-plate factor = $\frac{A_e}{A}$	1.42	1.16	1.04	1.07	1.24	1.48

TABLE II.- CALCULATION OF CONTRIBUTION OF VERTICAL TAIL TO DIRECTIONAL STABILITY BY PASS' METHOD OF REFERENCE 1 ($\alpha = 0^\circ$)



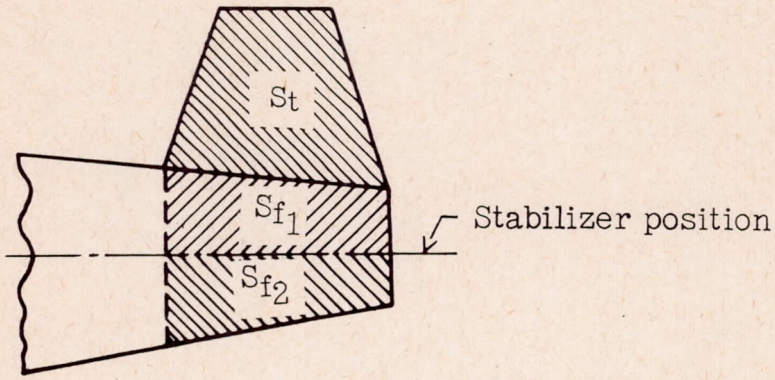
Stabilizer position	High	Middle	Low
Area, S_t, sq ft	2.41	3.01	3.61
Tail height, h_t, sq ft	1.79	2.13	2.48
Geometric aspect ratio, $A = \frac{h_t^2}{S_t}$	1.33	1.51	1.70
Effective aspect ratio, $A_e = 1.55A$ . . .	2.06	2.34	2.64
Normal-force-coefficient slope, $\left(C_{N_{\psi_t}}\right)_o$ (from fig. 3 of reference 1 with values increased 5 percent to account for absence of control-surface gap)	0.0464	0.0498	0.0531
Air-flow factor, $\frac{d(\psi - \sigma)(q/q_o)}{d\psi}$ (from reference 3)	0.94	0.94	0.94
Corrected normal-force-coefficient slope, $C_{N_{\psi_t}} = \left(C_{N_{\psi_t}}\right)_o$ (Air-flow factor)	0.0436	0.0469	0.0500
Contribution of vertical tail to directional stability, $C_{n_{\psi_t}} = -\left(\frac{S_t}{S_w}\right)\left(\frac{l}{b}\right)\left(C_{N_{\psi_t}}\right)$	-0.00144	-0.00193	-0.00248

TABLE III.- CALCULATION OF CONTRIBUTION OF VERTICAL TAIL TO DIRECTIONAL STABILITY BY LYONS AND BISGOOD'S METHOD OF REFERENCE 2 ($\alpha = 0^\circ$)



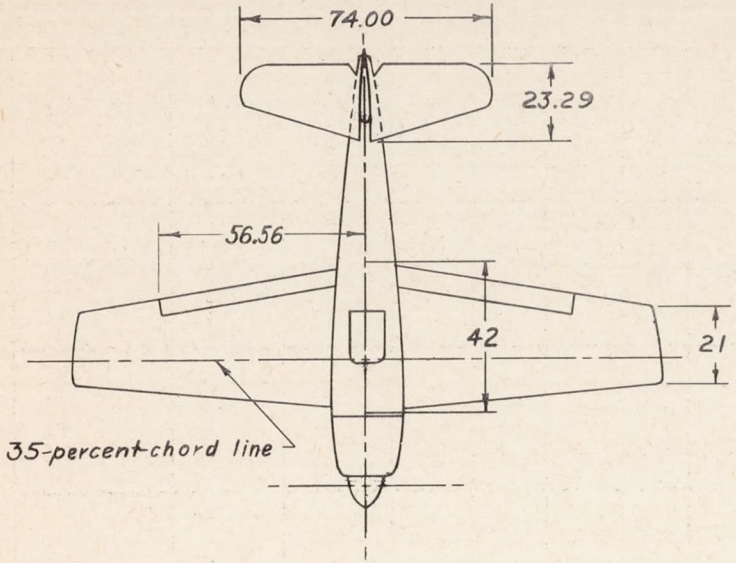
Stabilizer position	High	Middle	Low
Tail area, S_t, sq ft	3.84	3.84	3.84
Tail height, h_t, ft	2.65	2.65	2.65
Height to stabilizer, h_1, ft	1.79	2.14	2.48
h_1/h_t	0.675	0.807	0.936
Geometric aspect ratio, $A = \frac{h_t^2}{S_t}$	1.83	1.83	1.83
A_e/A (amended fig. 9(b) of reference 2)	1.06	1.19	1.36
Effective aspect ratio, A_e	1.94	2.18	2.49
Trailing-edge angle (approx.), deg	14.0	14.0	14.0
Control-gap size	None	None	None
Vertical-tail taper ratio, $\frac{\text{Root chord}}{\text{Tip chord}}$	2.08	2.08	2.08
Slope $a_1 = C_{N_\psi}$ for isolated three-dimensional surface (fig. 10 of reference 2)	0.0471	0.0506	0.0551
Fuselage height, h_f, ft	1.1	1.1	1.1
h_f/h_t	0.415	0.415	0.415
Interference correction factor, a_1'/a_1 (fig. 12(a) of reference 2, interpolated for low midwing)	0.66	0.66	0.66
$C_{N_{\psi_t}} = a_1'$, per deg	0.0311	0.0334	0.0364
Contribution of vertical tail to directional stability, $C_{n_{\psi_t}} = -\left(\frac{S_t}{S_w}\right)\left(\frac{l}{b}\right)\left(C_{N_{\psi_t}}\right)$	-0.00164	-0.00175	-0.00191

TABLE IV.- CONTRIBUTION OF COMPONENTS OF TAIL-FUSELAGE COMBINATION AS IMPLIED BY REFERENCE 2 (LYONS AND BISGOOD)



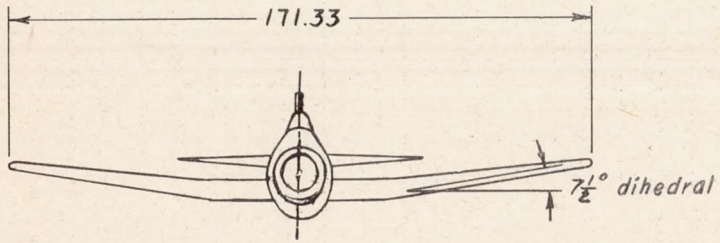
Stabilizer position	High	Middle	Low
S_t, tail area	2.04	2.04	2.04
S_{f_1}, fuselage area above stabilizer . .	0.37	0.97	1.57
S_{f_2}, fuselage area below stabilizer . .	1.43	0.83	0.23
$S_{total} = S_t + S_{f_1} + S_{f_2}$	3.84	3.84	3.84
$C_{N_{\psi_t}}$ based on area S_{total}	0.0311	0.0334	0.0364
$C_{N_{\psi_t}}$ based on area S_t	0.0585	0.0629	0.0685
Contribution of vertical-tail area, $C_{N_{\psi_t}}$, based on area S_t	0.0311	0.0334	0.0364
Contribution of fuselage area above stabilizer, $C_{N_{\psi_{f_1}}}$, based on area S_t .	0.0056	0.0159	0.0280
Contribution of fuselage area below stabilizer, $C_{N_{\psi_{f_2}}}$, based on area S_t	0.0218	0.0136	0.0041

NACA



Areas

Wing, sq ft	37.12
Wing flap, sq ft	4.42
Horizontal tail, sq ft	8.65



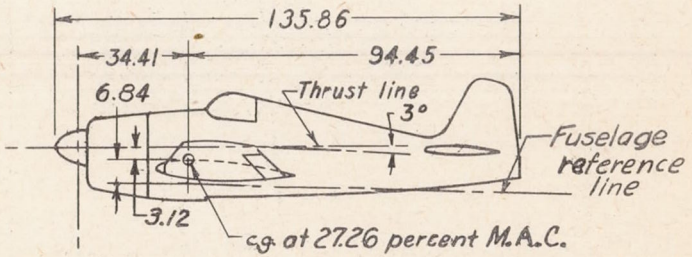


Figure 1.- Three-view drawing of the $\frac{1}{3}$-scale model of a conventional low-wing fighter airplane. (All dimensions are given in inches.)

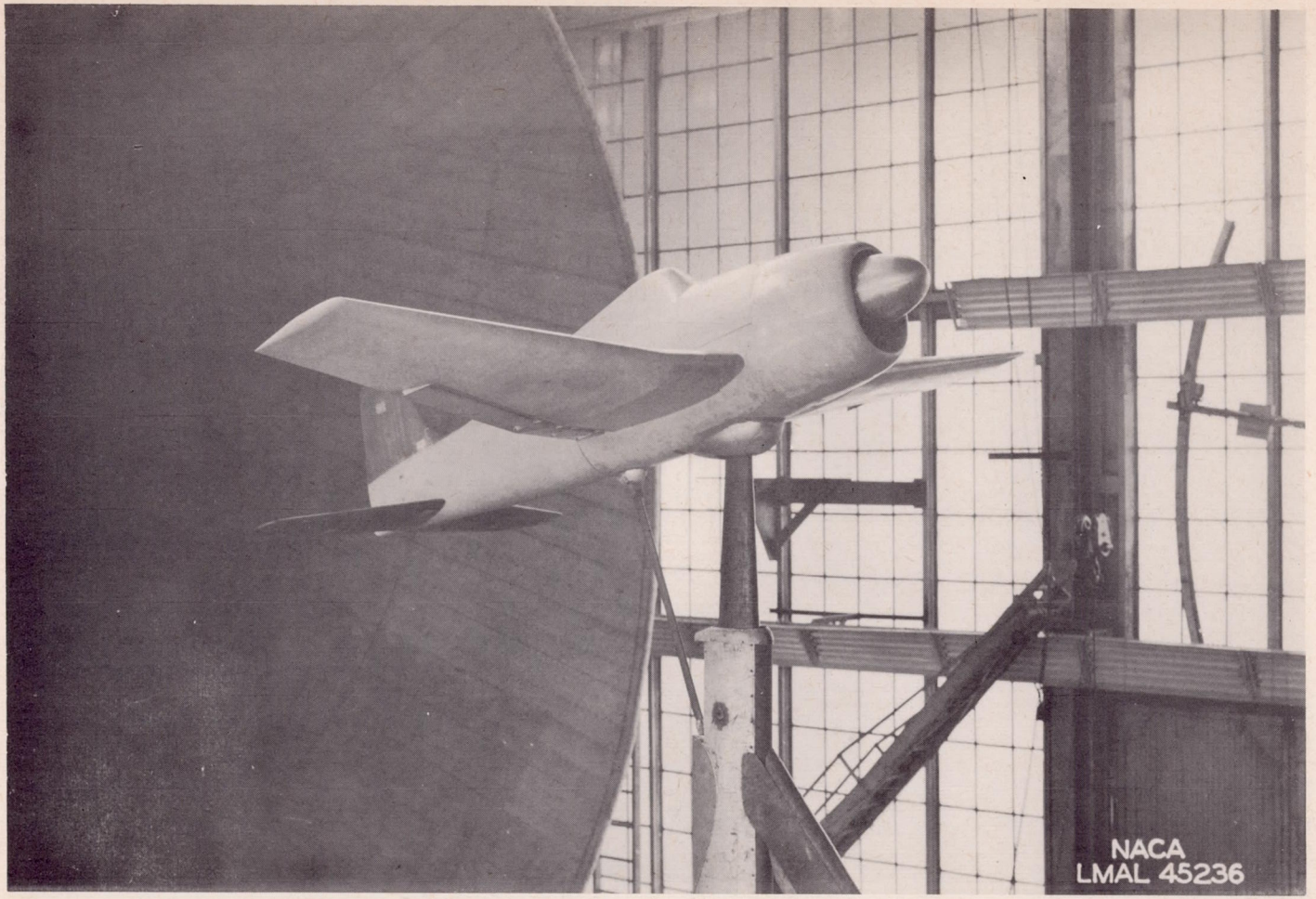


Figure 2.- Photograph of $\frac{1}{3}$-scale model of conventional low-wing fighter airplane mounted in Langley propeller-research tunnel. Stabilizer in low position.

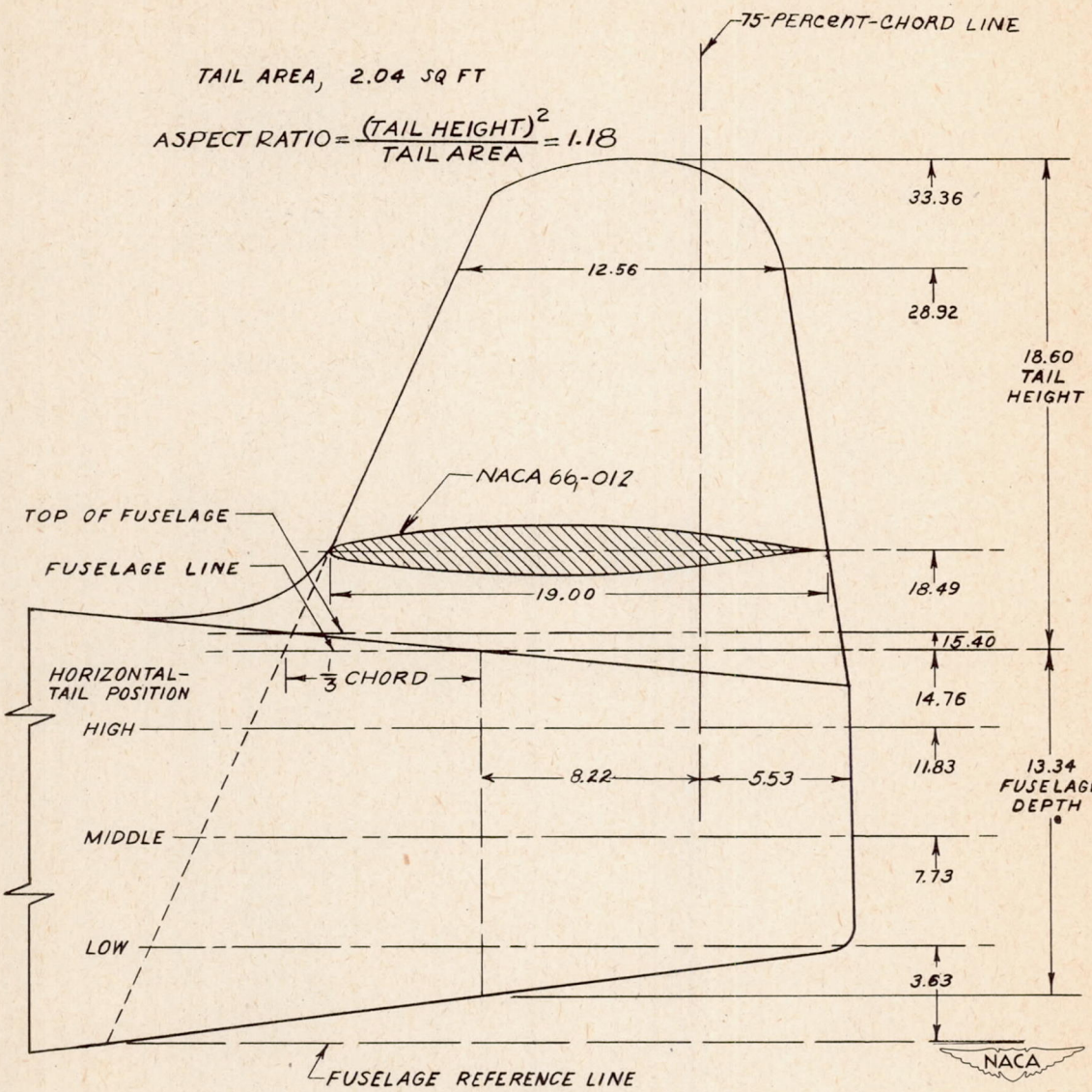


Figure 3.- Sketch showing details of vertical tail. (All dimensions are given in inches.)

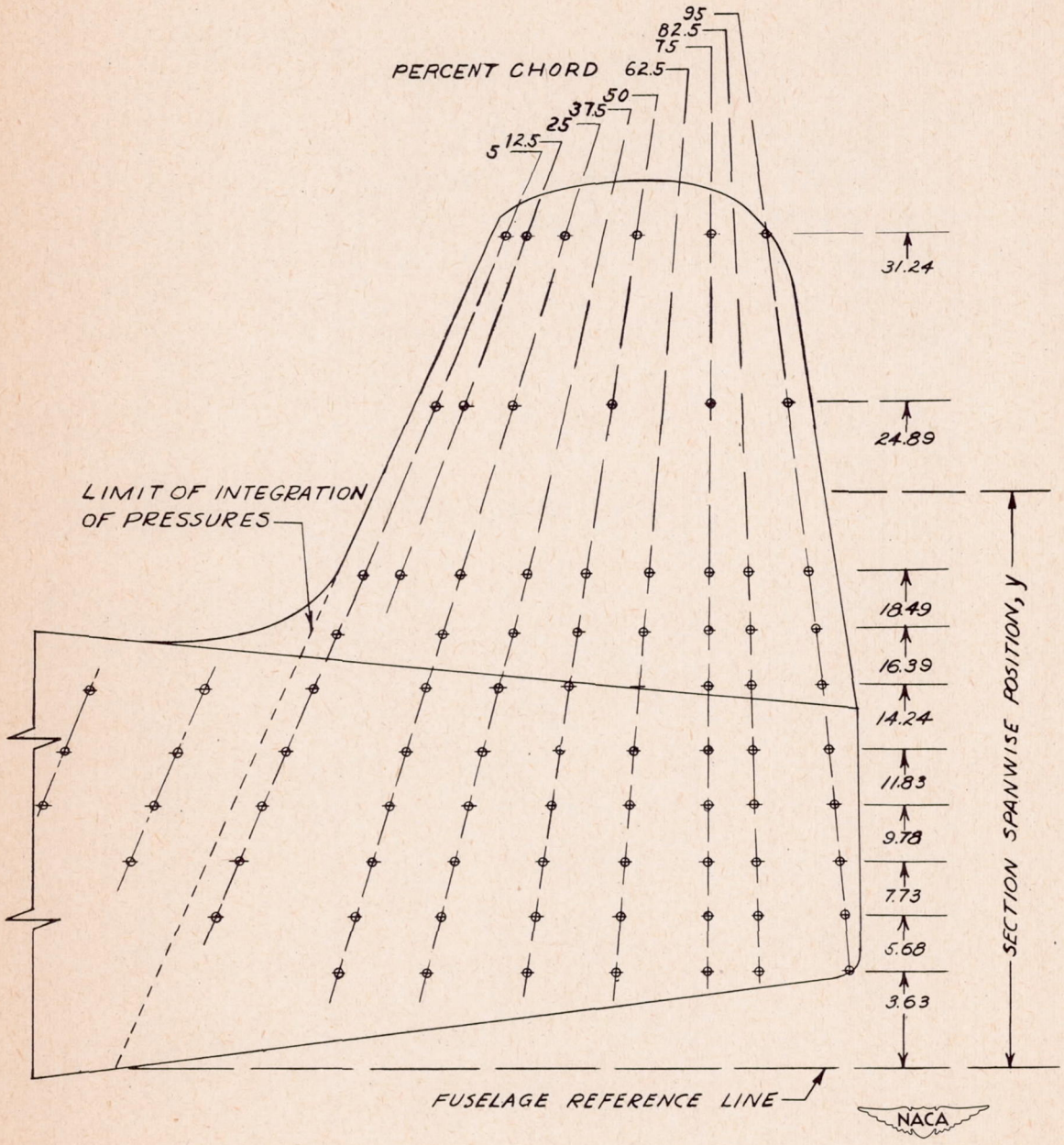


Figure 4.- Orifice distribution on each side of vertical tail and fuselage. (All dimensions are given in inches.)

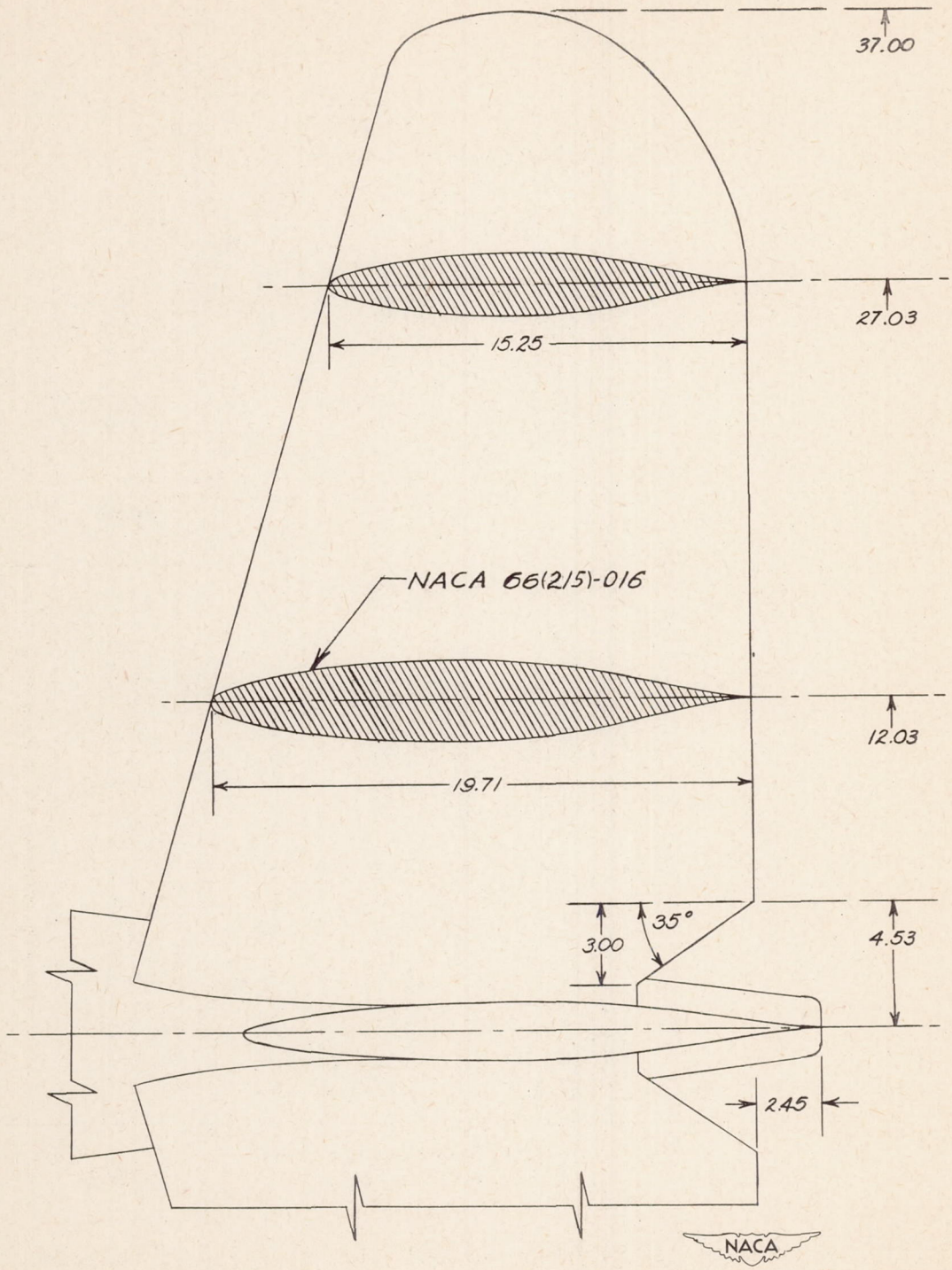


Figure 5.- Sketch showing details of horizontal tail in high position. (All dimensions are given in inches.)

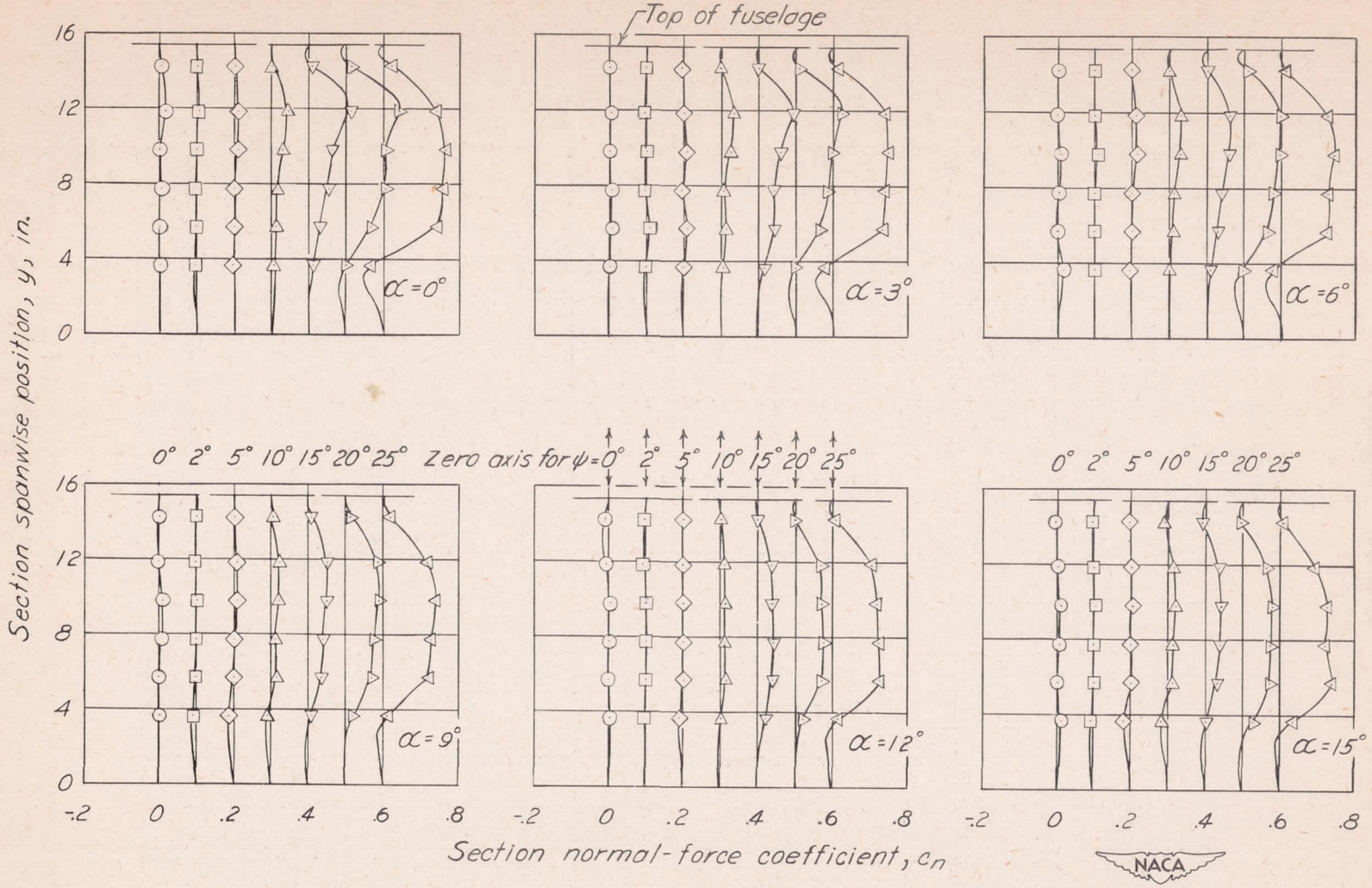
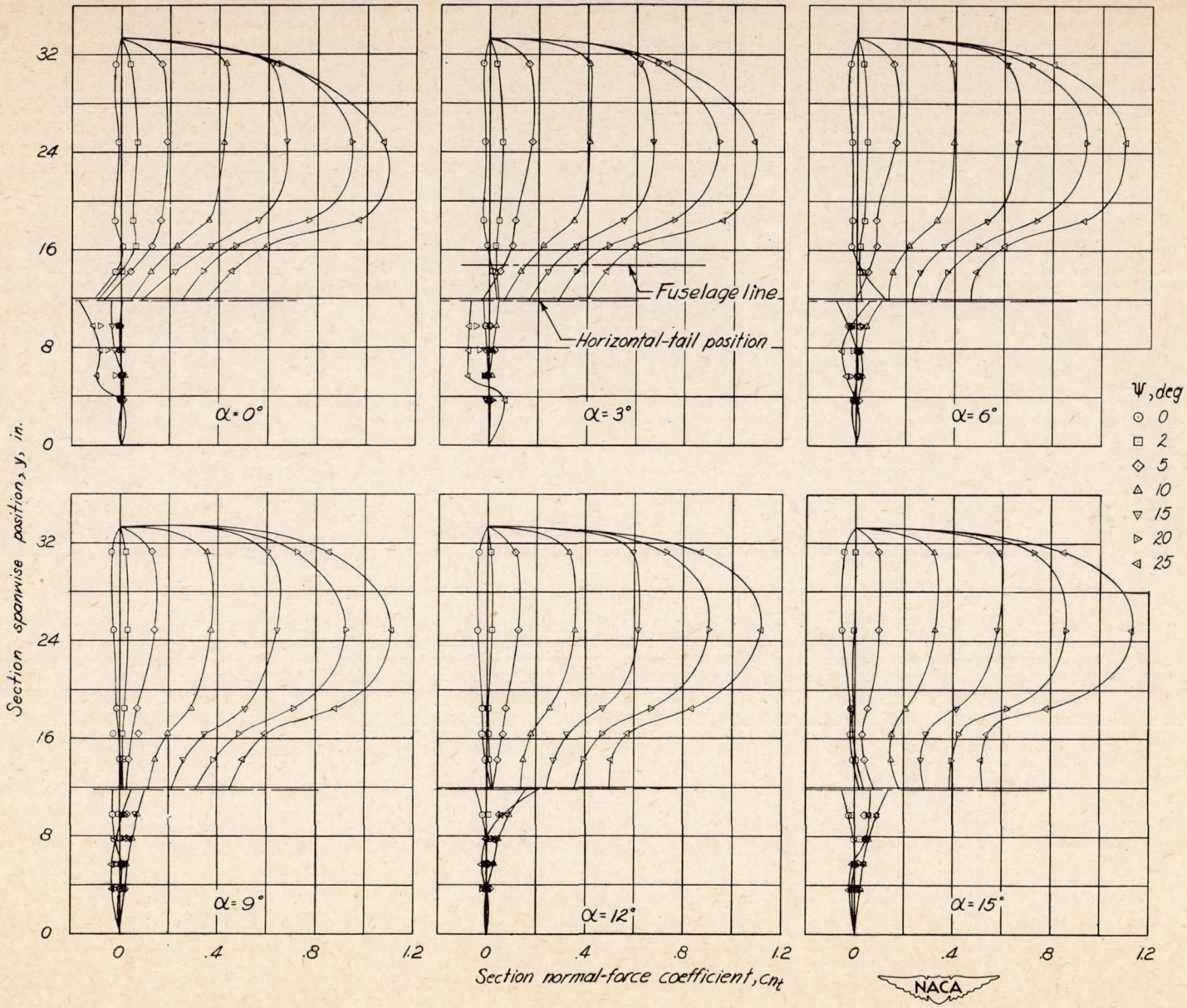
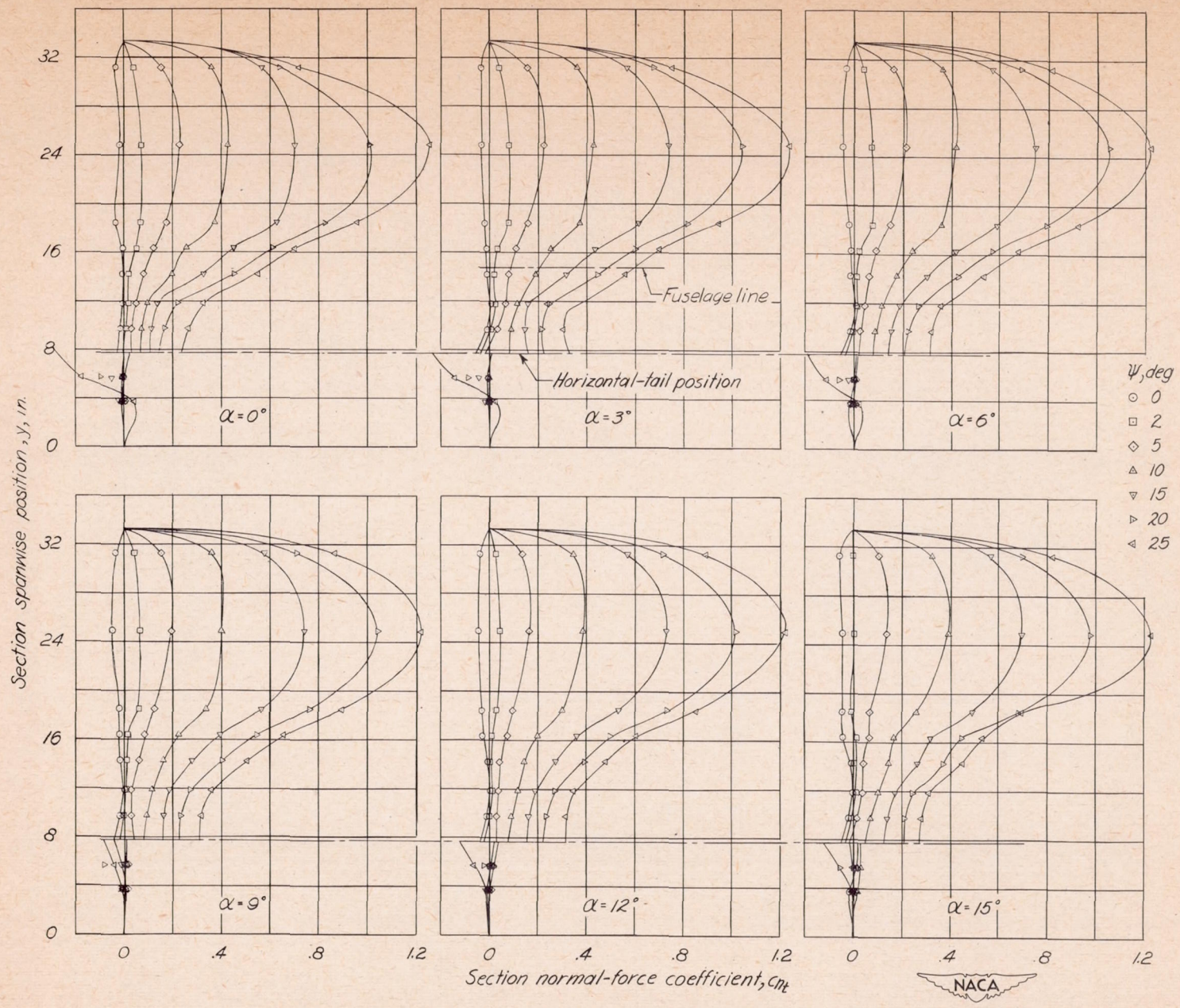


Figure 6.- Fuselage section normal-force coefficient as a function of section spanwise position with angle of attack and angle of yaw as parameters. Vertical and horizontal tails removed.

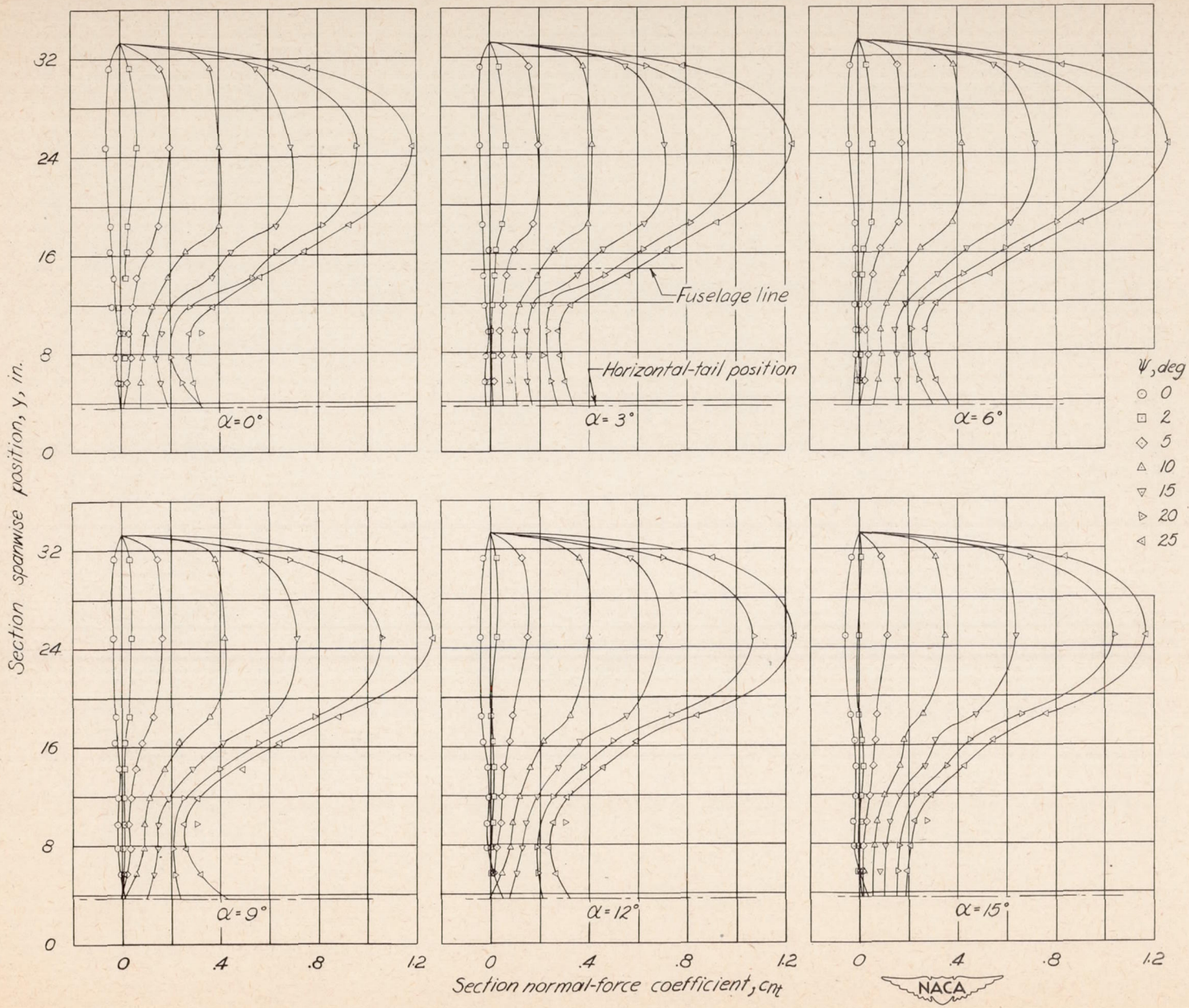


(a) Horizontal tail in high position.

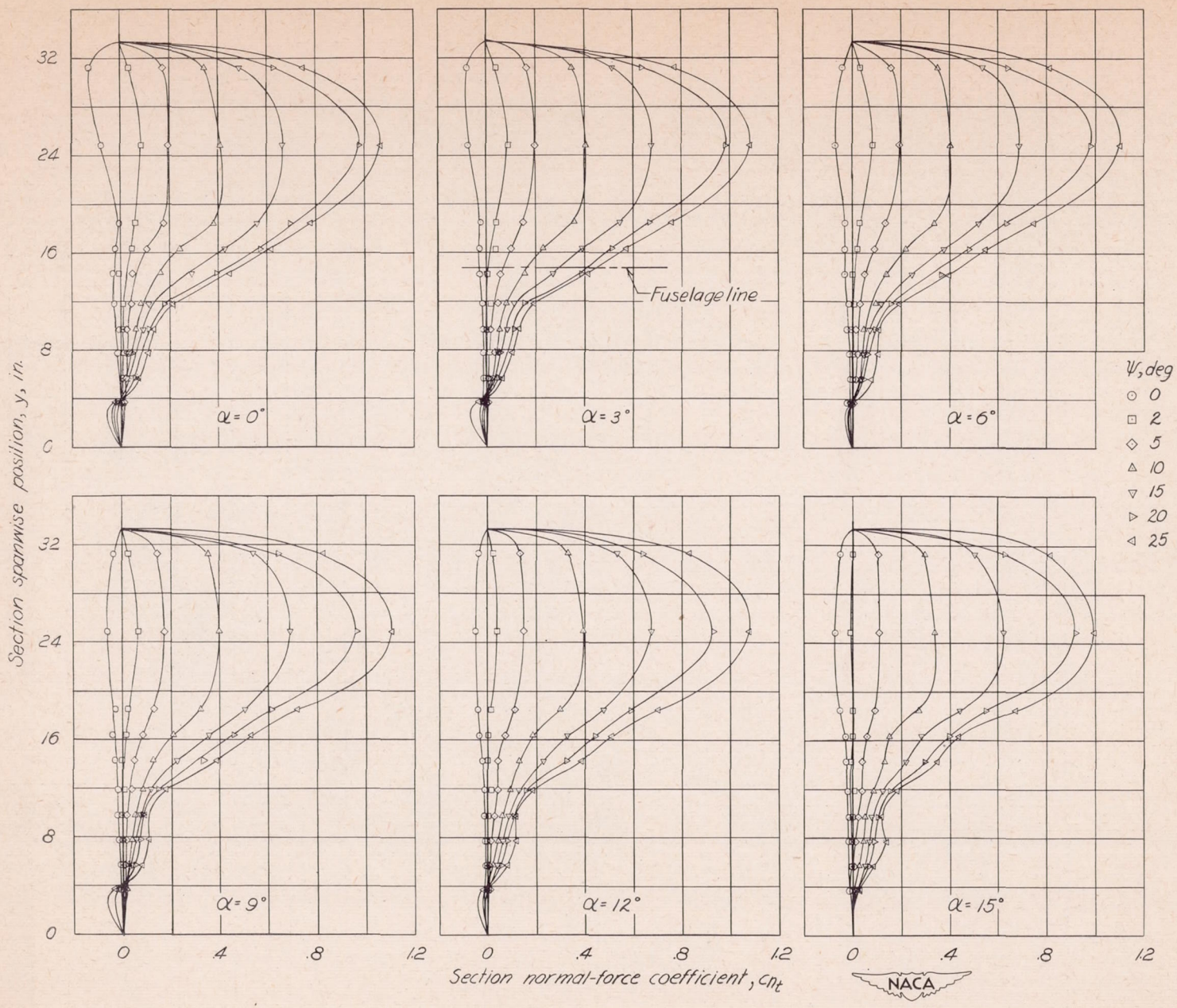
Figure 7.- Vertical-tail section normal-force coefficient as a function of section spanwise position with angle of attack and angle of yaw as parameters.



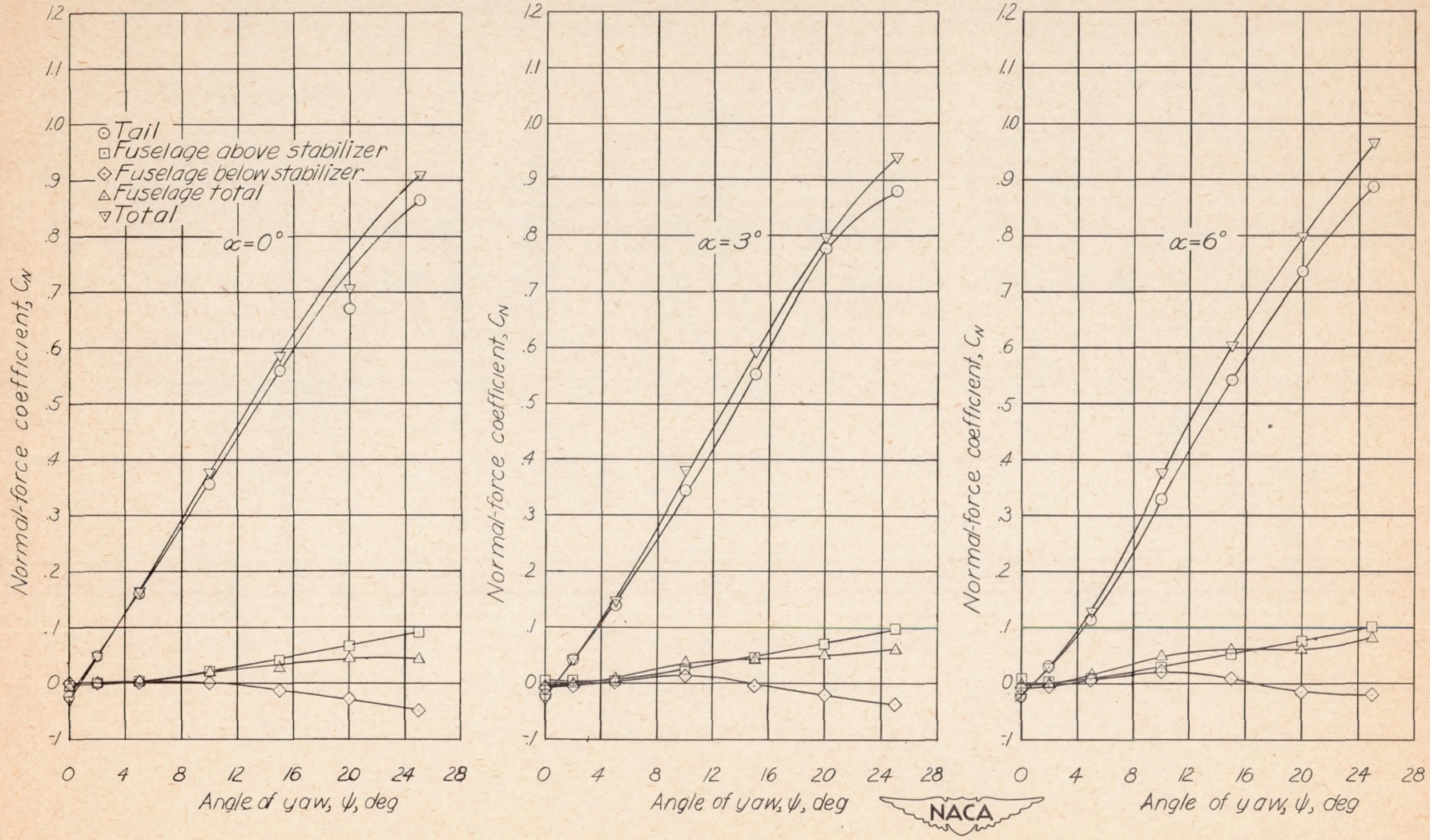
(b) Horizontal tail in middle position.
Figure 7.- Continued



(c) Horizontal tail in low position.
Figure 7.- Continued

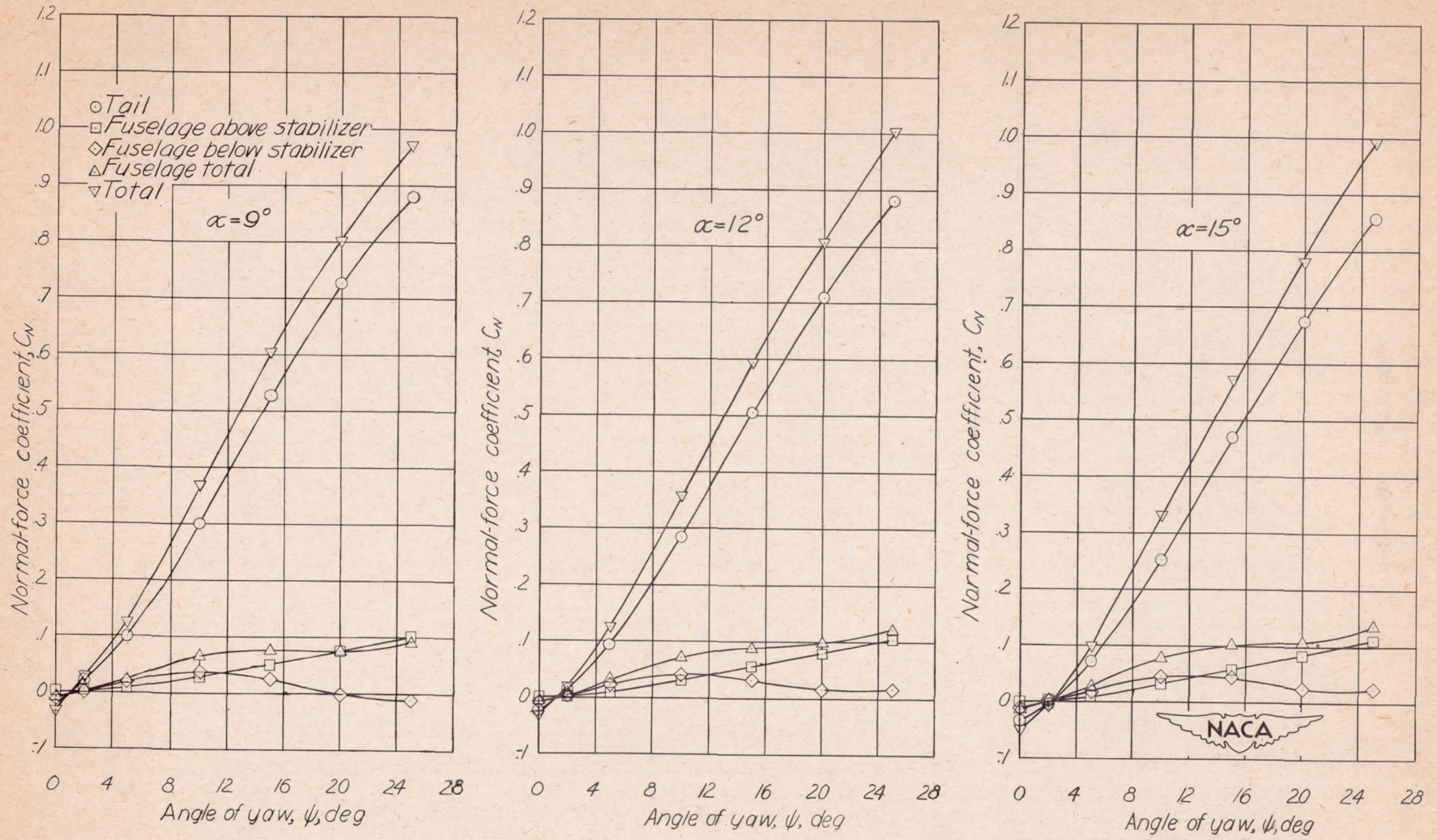


(d) Horizontal tail removed.
Figure 7.- Concluded.

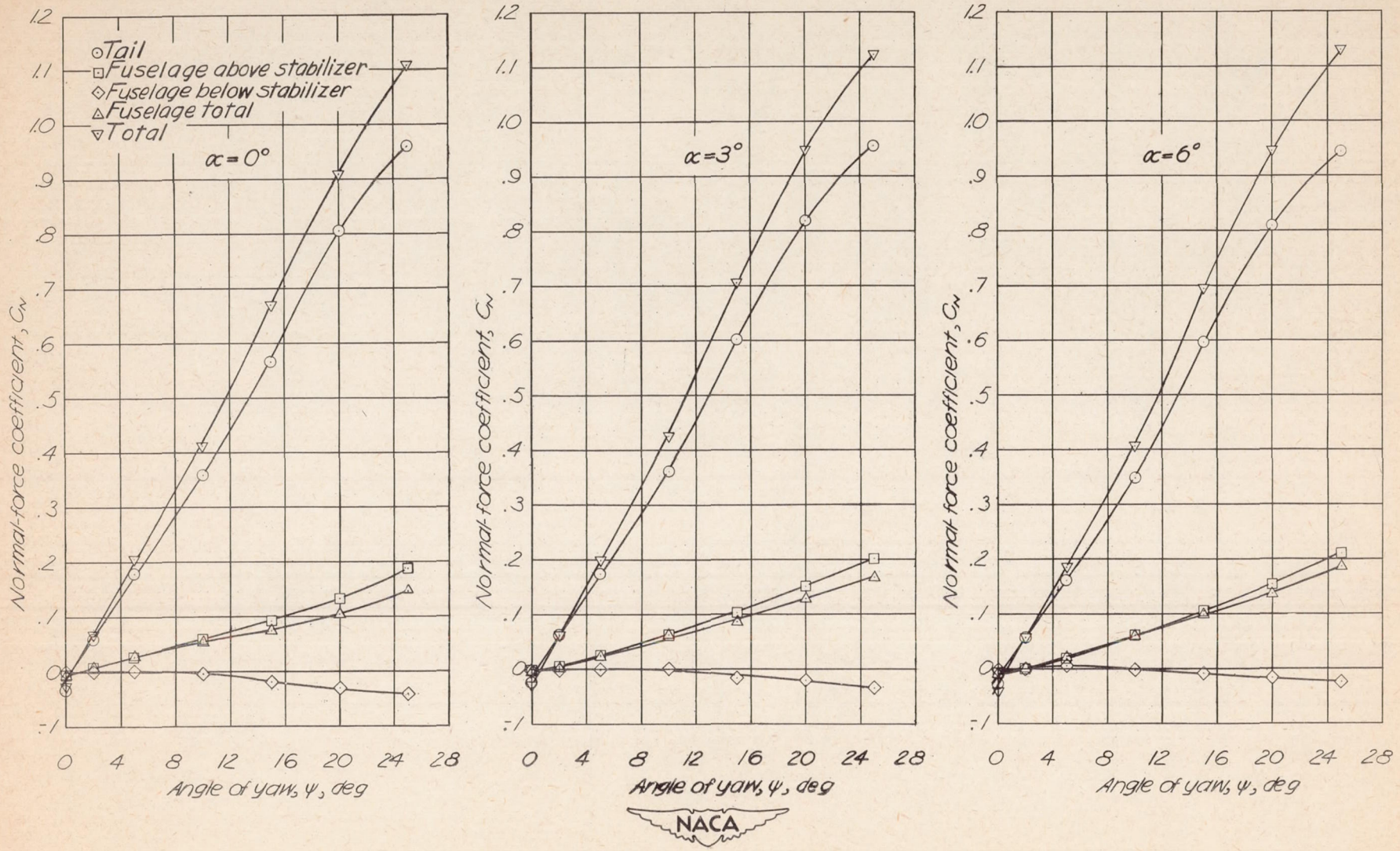


(a) Horizontal tail in high position.

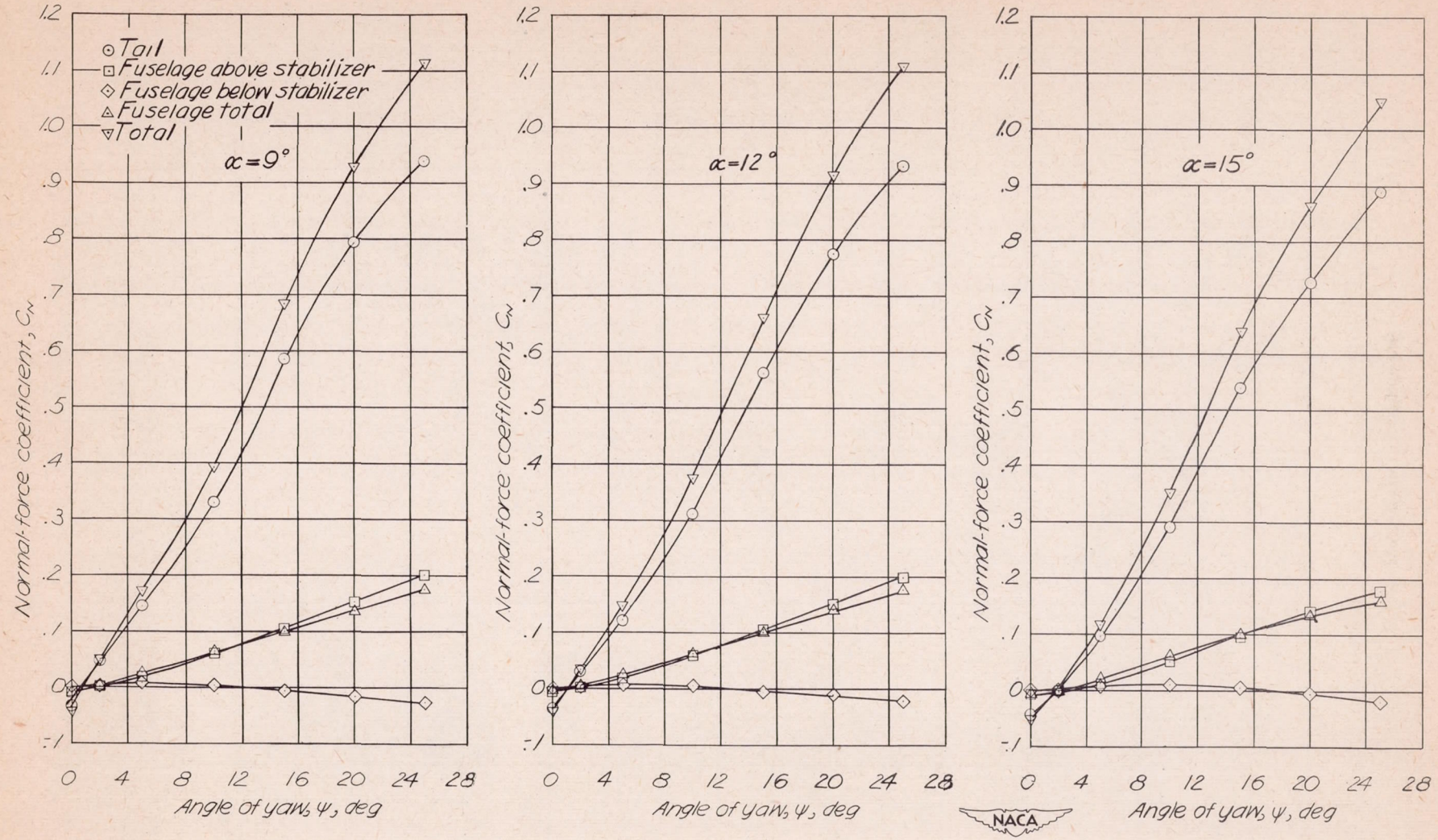
Figure 8.- Variation of normal-force coefficient with angle of yaw for components of the tail-fuselage combination.



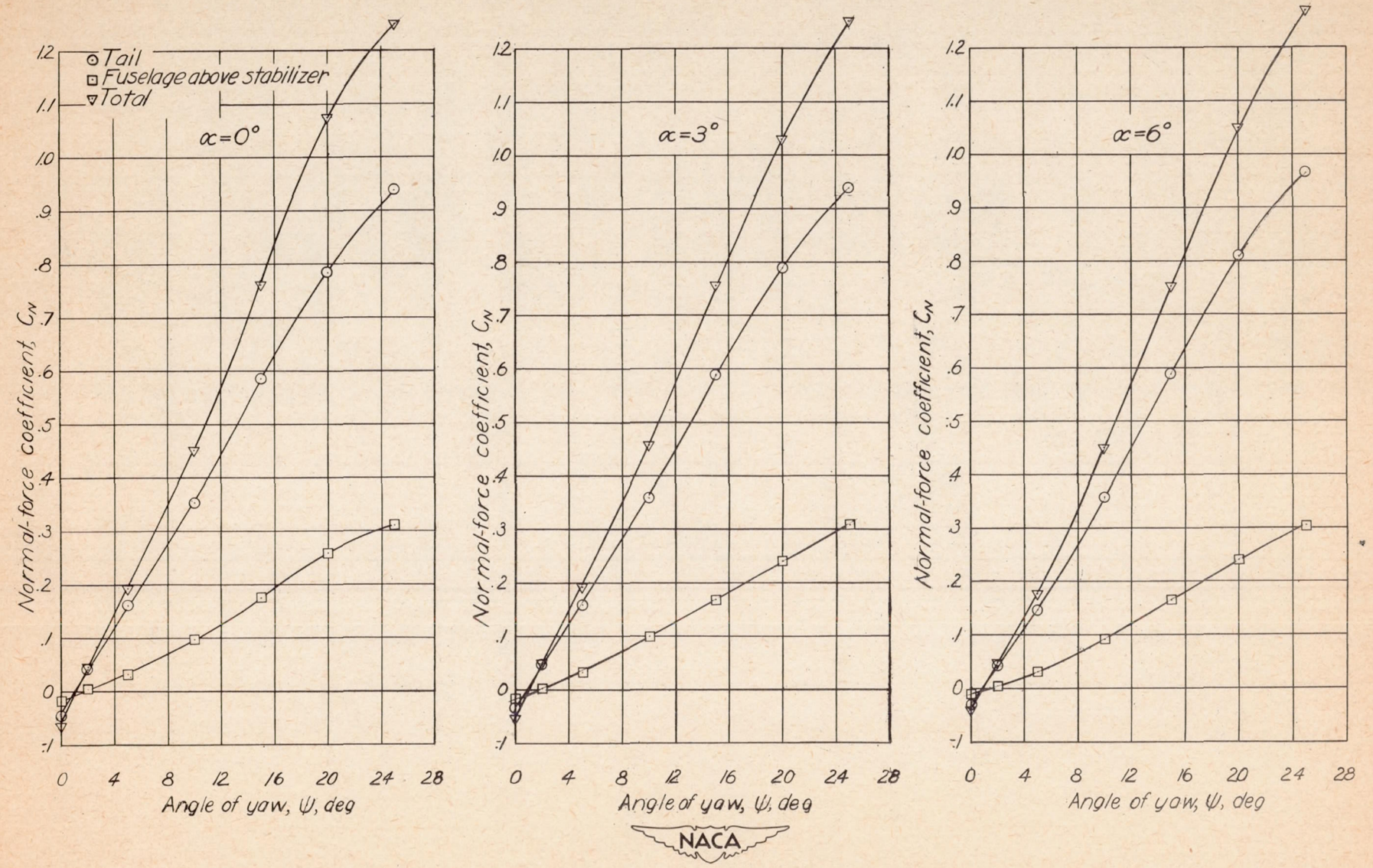
(a) Concluded.
Figure 8.- Continued.



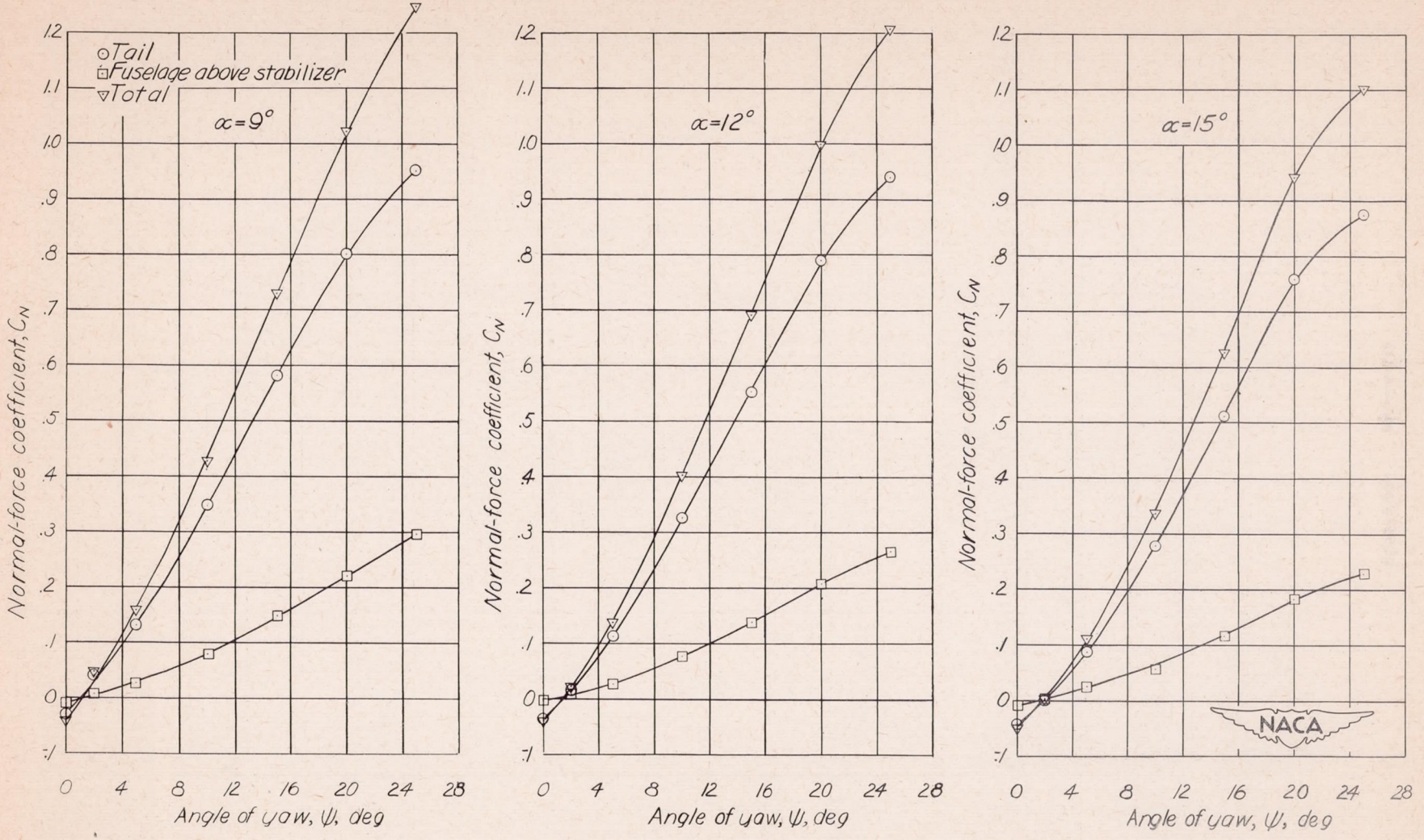
(b) Horizontal tail in middle position.
Figure 8.- Continued.



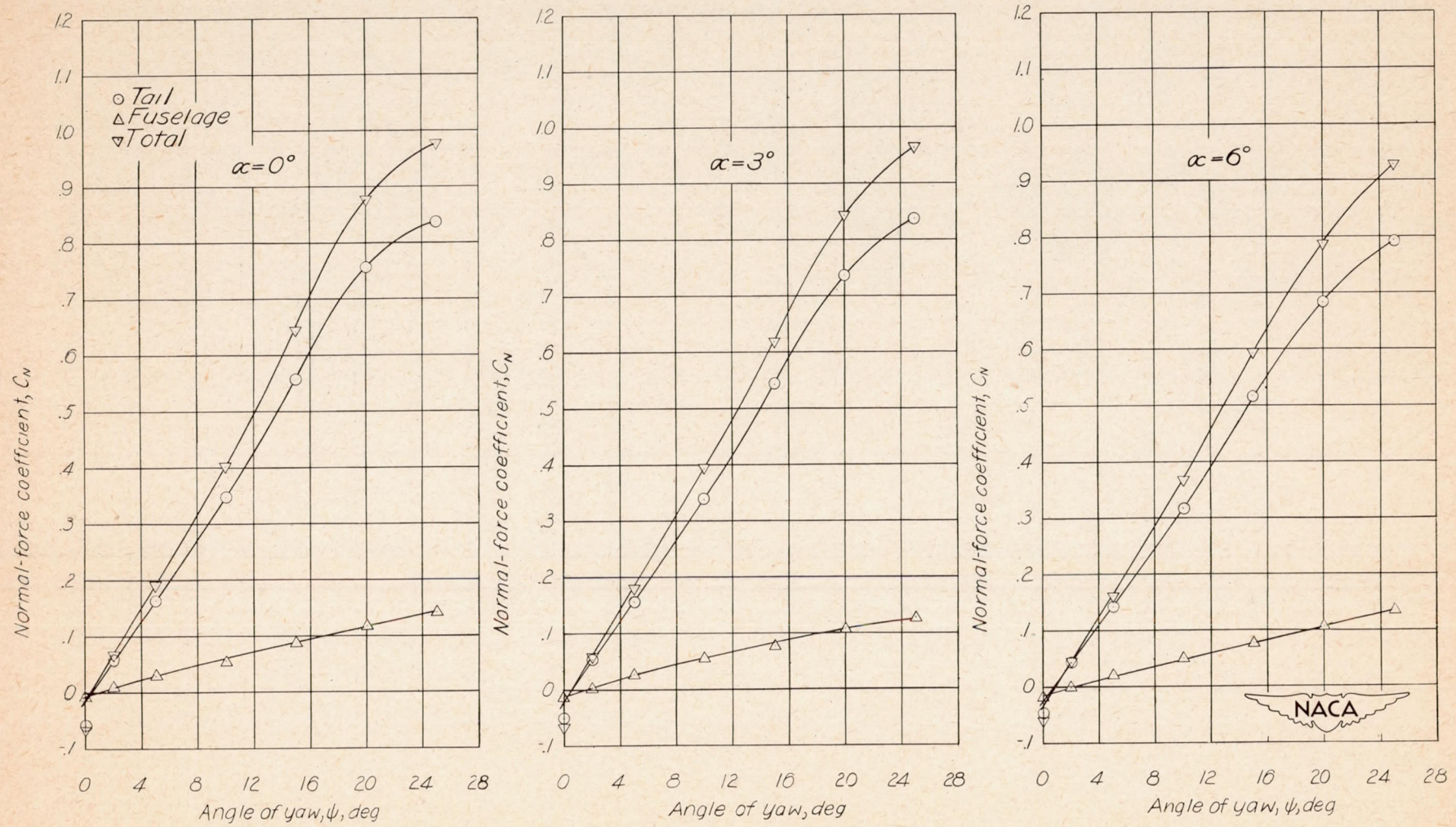
(b) Concluded.
Figure 8.- Continued.



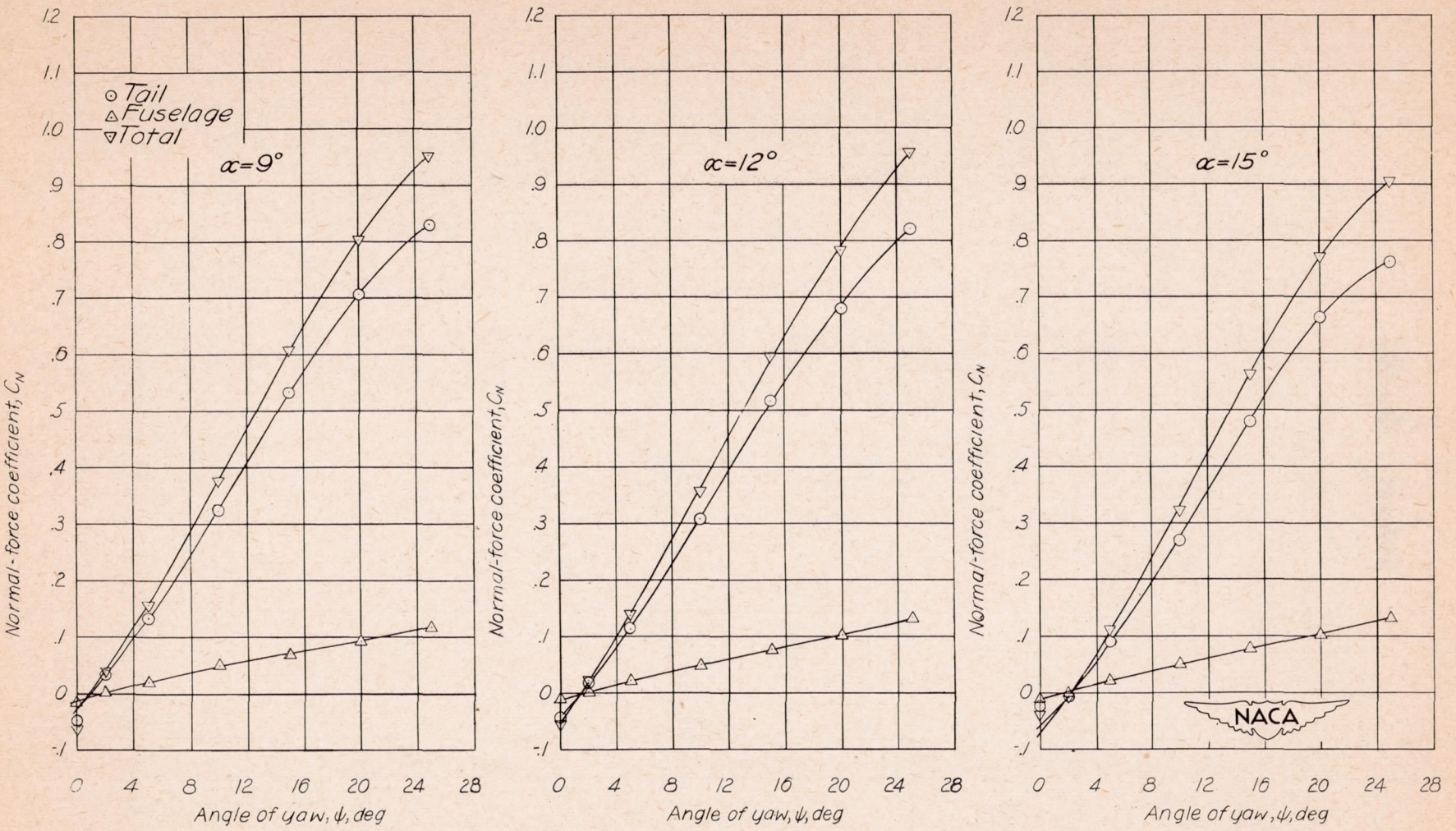
(c) Horizontal tail in low position.
Figure 8.- Continued.



(c) Concluded.
Figure 8.- Continued.



(d) Horizontal tail removed.
Figure 8.- Continued.



(d) Concluded.
Figure 8.- Concluded.

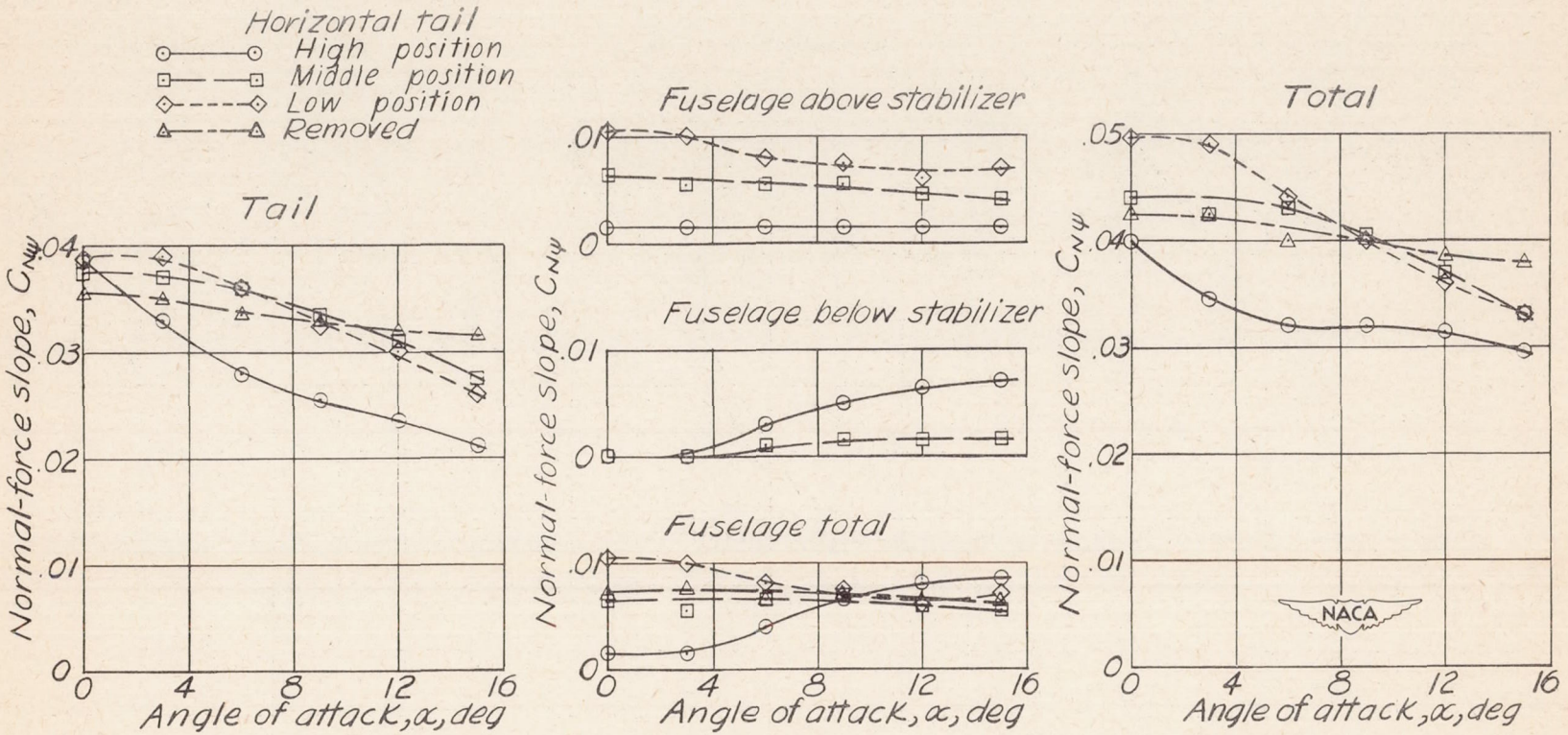


Figure 9.- Variation of normal-force slope with angle of attack for components of the tail-fuselage combination.

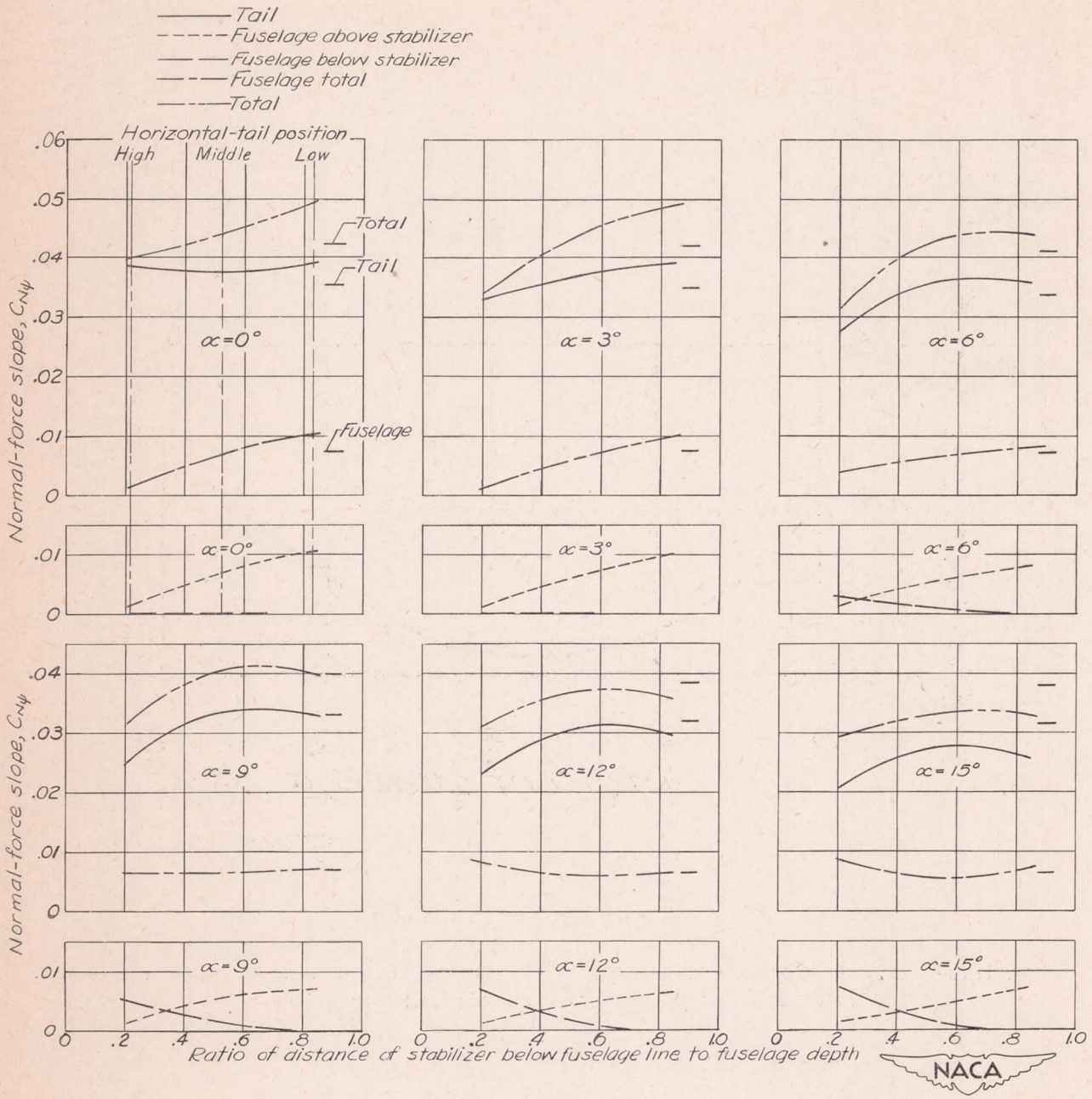


Figure 10.- Variation of normal-force slope with stabilizer position for components of the tail-fuselage combination. Short dash on right side of each curve indicates the corresponding value obtained with the horizontal tail removed.

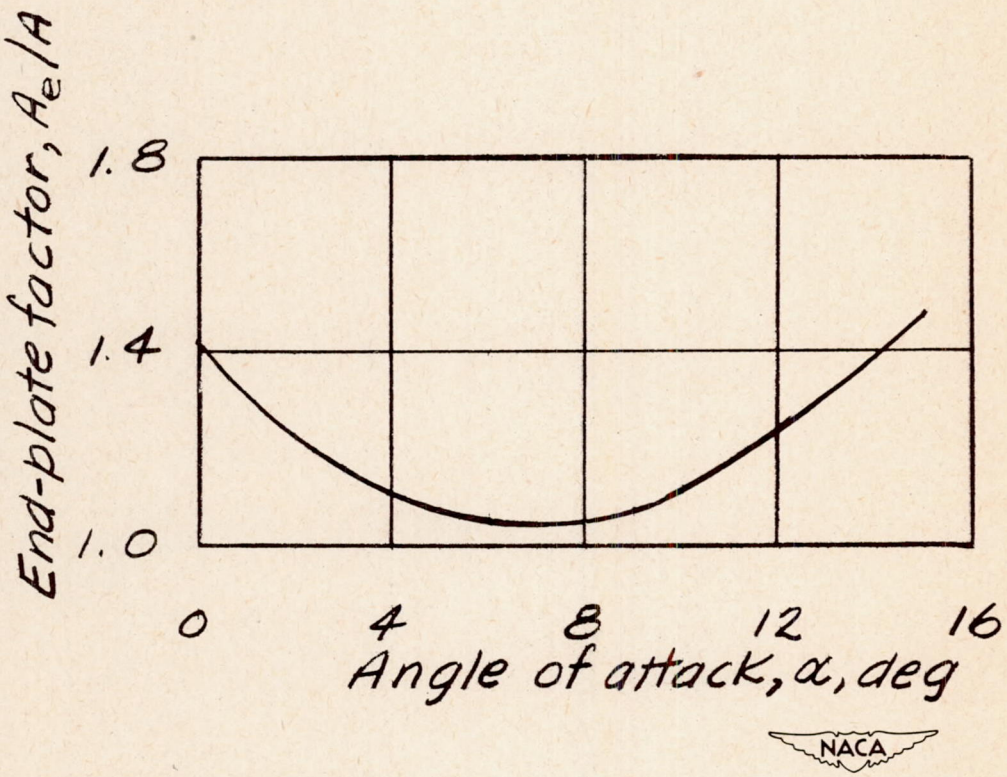


Figure 11.- Variation of end-plate factor with angle of attack for vertical tail with high stabilizer position.

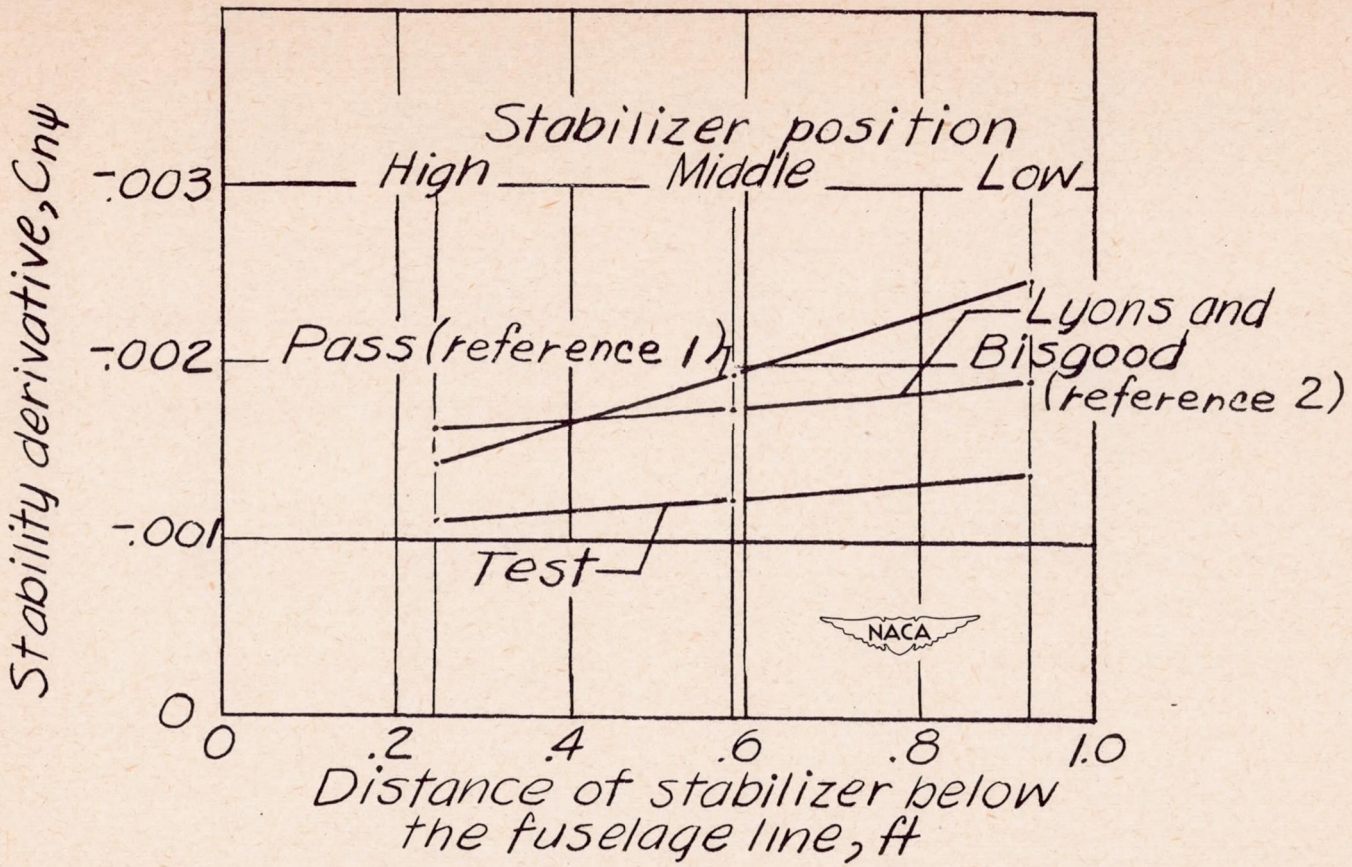


Figure 12.- Comparison of the measured stability derivative with those calculated by Pass' method (reference 1) and Lyons and Bisgood's method (reference 2).

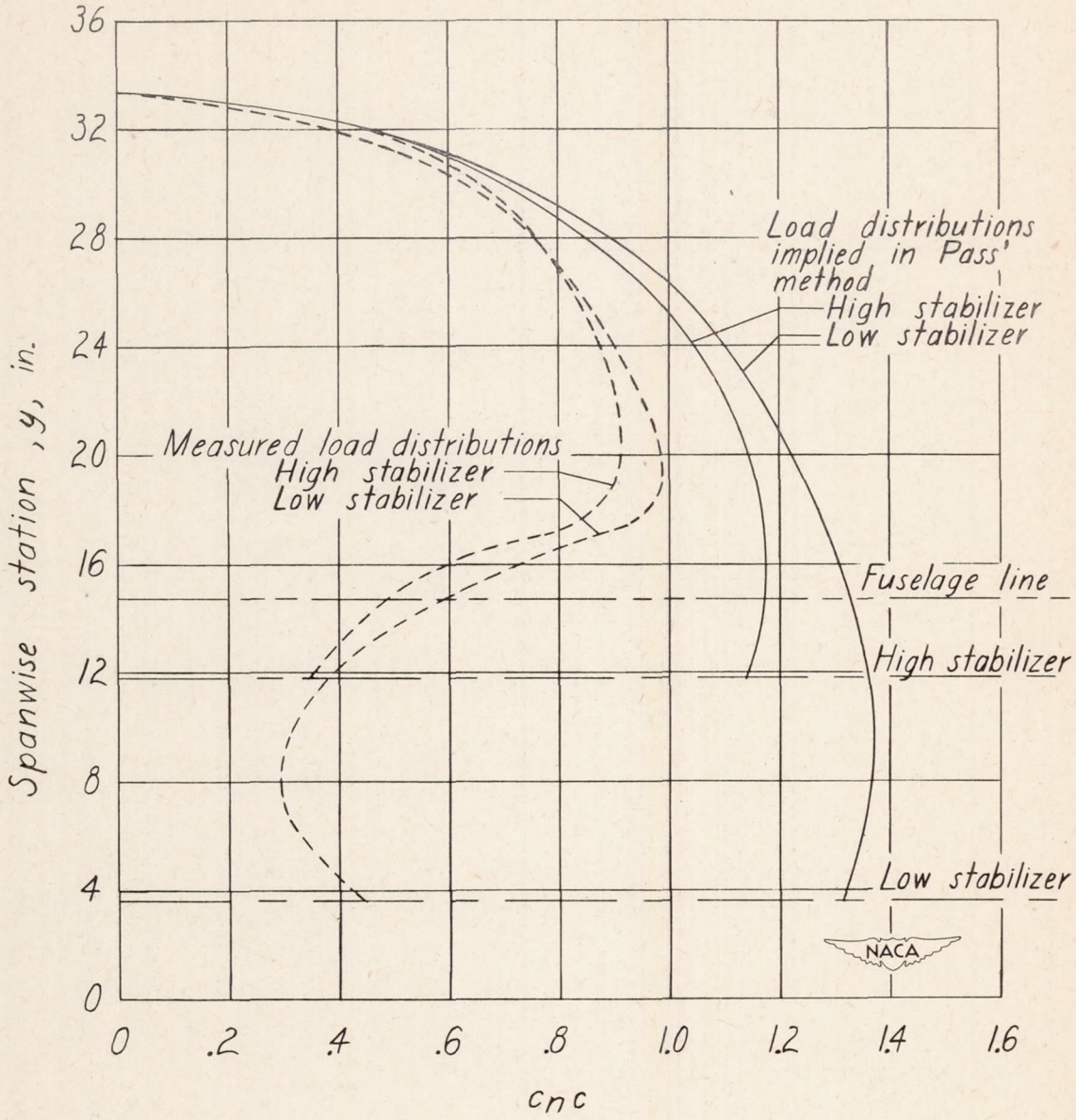


Figure 13.- Comparison of the measured load distributions with those implied in Pass' method. $\alpha = 0^{\circ}$; $\psi = 15^{\circ}$.

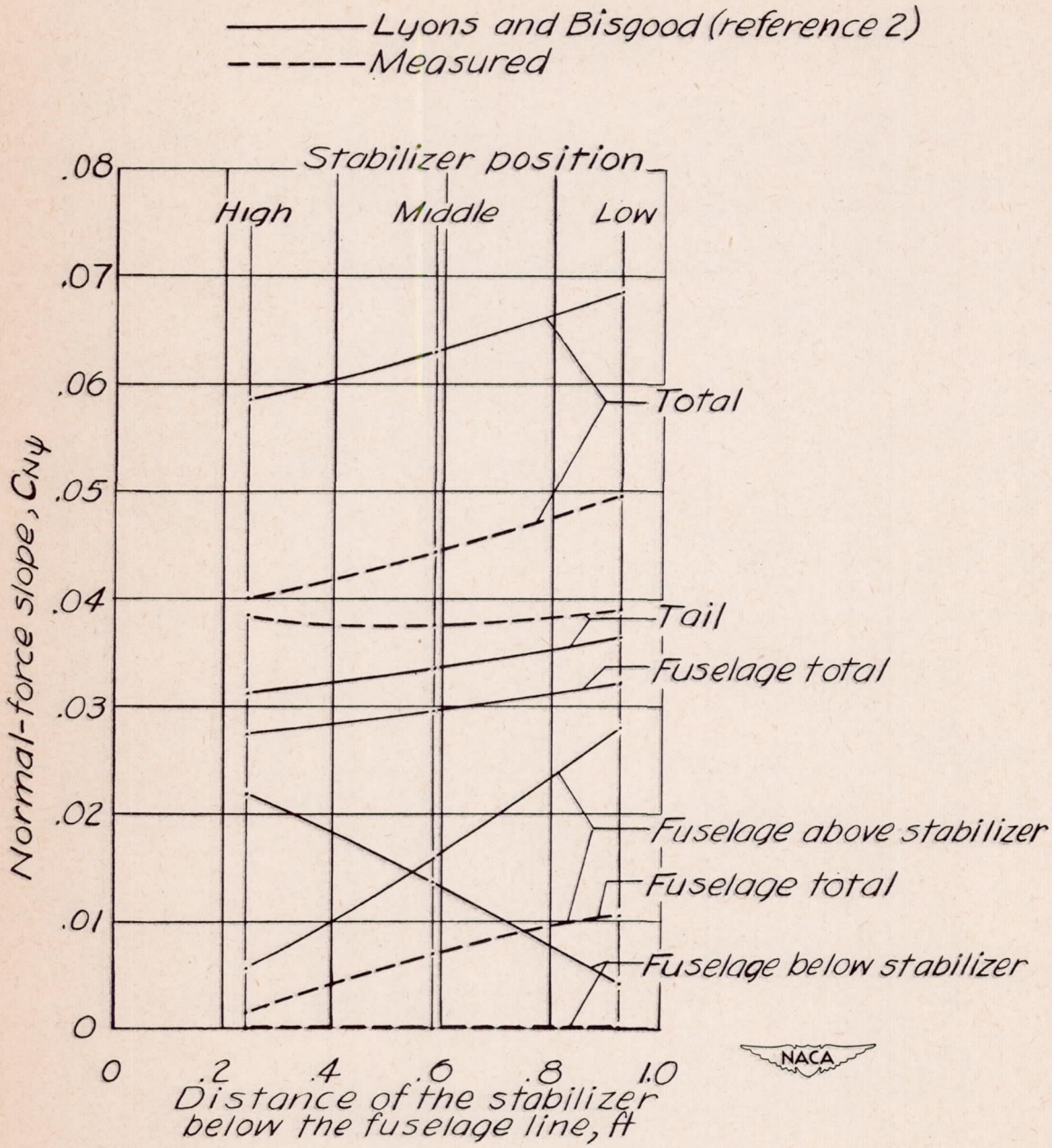


Figure 14.- Comparison of the measured component contributions with those calculated as implied in the method of Lyons and Bisgood (reference 2). $\alpha = 0^\circ$.